

# Expected information gain estimation via density approximations: Sample allocation and dimension reduction

Fengyi Li\*, Ricardo Baptista†, and Youssef Marzouk\*

**Abstract.** Computing expected information gain (EIG) from prior to posterior (equivalently, mutual information between candidate observations and model parameters or other quantities of interest) is a fundamental challenge in Bayesian optimal experimental design. We formulate flexible transport-based schemes for EIG estimation in general nonlinear/non-Gaussian settings, compatible with both standard and implicit Bayesian models. These schemes are representative of two-stage methods for estimating or bounding EIG using marginal and conditional density estimates. In this setting, we analyze the optimal allocation of samples between training (density estimation) and approximation of the outer prior expectation. We show that with this optimal sample allocation, the mean squared error (MSE) of the resulting EIG estimator converges more quickly than that of a standard nested Monte Carlo scheme. We then address the estimation of EIG in high dimensions, by deriving gradient-based upper bounds on the mutual information lost by projecting the parameters and/or observations to lower-dimensional subspaces. Minimizing these upper bounds yields projectors and hence low-dimensional EIG approximations that outperform approximations obtained via other linear dimension reduction schemes. Numerical experiments on a PDE-constrained Bayesian inverse problem also illustrate a favorable trade-off between dimension truncation and the modeling of non-Gaussianity, when estimating EIG from finite samples in high dimensions.

**Key words.** Optimal experimental design, expected information gain, mutual information, density estimation, transportation of measure, dimension reduction

**AMS subject classifications.** 62K05, 62B10, 62G07, 62F15

**1. Introduction.** Optimal experimental design (OED) problems are ubiquitous in the physical and biological sciences, engineering, social sciences, and beyond [32, 1, 38, 46, 68]. The goal of OED is to identify observational or experimental configurations that are—in a specific sense defined by the experimenter—most useful, before the associated data are collected. Most OED approaches begin with a parametric statistical model for the observations and seek a design that maximizes, for example, a notion of *information gain* or uncertainty reduction in the model’s parameters, or another utility that reflects a downstream task in which the parameters are involved. Typically these objectives can be maximized only in expectation over the data.

To make this idea concrete, let the observations associated with some candidate design be represented as a random vector  $Y$  taking values in  $\mathbb{R}^{n_y}$ , such that our parametric statistical model is specified by conditional probability density functions<sup>1</sup> of  $Y$ ,  $\pi_{Y|X,d}(\cdot|x,d)$ , for parameter values  $x \in \mathbb{R}^{n_x}$  and design parameters  $d \in \Xi$ . We work in the Bayesian setting, such that the parameters  $x$  are treated as a random vector  $X$  and endowed with a prior density  $\pi_X$ . The posterior density of  $X$  for observations  $y$  is given by Bayes’ rule as

$$(1.1) \quad \pi_{X|Y,d}(x|y,d) = \frac{\pi_{Y|X,d}(y|x,d) \pi_X(x)}{\pi_{Y|d}(y|d)}.$$

Here, the marginal density of the observations  $\pi_{Y|d}$  is also called the evidence or marginal likelihood. In the Bayesian paradigm, the prior and posterior distributions represent, respectively, our states

---

\*Aeronautics and Astronautics, Massachusetts Institute of Technology ([fengyil@mit.edu](mailto:fengyil@mit.edu), [ymarz@mit.edu](mailto:ymarz@mit.edu)).

†Computing and Mathematical Sciences, California Institute of Technology ([rsb@caltech.edu](mailto:rsb@caltech.edu))

<sup>1</sup>Here and throughout the paper, we assume that all distributions are absolutely continuous with respect to Lebesgue measure, so that these Lebesgue densities exist.

of knowledge before and after having observed  $Y = y$ . We always assume that the prior density of  $X$  is functionally independent of the design  $d$ .

In the special case of linear-Gaussian models, i.e.,  $Y|x, d \sim \mathcal{N}(G(d)x, \Sigma_{Y|X})$  for some design-dependent matrix  $G(d) \in \mathbb{R}^{n_y \times n_x}$  and covariance matrix  $\Sigma_{Y|X}$ , the classical ‘‘alphabetic optimality’’ criteria are simply functions of the Fisher information matrix  $G(d)^\top \Sigma_{Y|X}^{-1} G(d)$  of the model, which is independent of  $x$ . For example, choosing  $d$  to maximize the trace of the Fisher information matrix (A-optimality) is a natural criterion if one would like to minimize the variance of parameter estimates on average for any observation; similarly, maximizing the determinant of the Fisher information (D-optimality) minimizes the volume of the confidence ellipsoid [15]. In the *Bayesian* linear-Gaussian setting, these alphabetic optimality criteria can be modified to include the prior: for instance, Bayesian D-optimality then seeks to minimize the determinant of the posterior covariance, and so on.

In the nonlinear setting, the Fisher information matrix—and the Hessian of the log-posterior density—depend on the parameters  $x$ , and thus these simple alphabetic optimality criteria do not directly apply. Many have suggested averaging these criteria over the parameter space, leading to a variety of nonlinear design heuristics [22, 52] which in some cases permit interesting information theoretic interpretations [65, 48, 51]. A more general and principled approach, however, is to consider the *expected information gain* (EIG) from prior to posterior, i.e.,

$$(1.2) \quad \text{EIG}(d) := \mathbb{E}_{Y|d} \left[ \mathcal{D}_{\text{KL}}(\pi_{X|Y,d} \parallel \pi_X) \right],$$

where  $\mathcal{D}_{\text{KL}}$  denotes the Kullback–Leibler (KL) divergence. This design objective was advocated by [41] as a natural measure of information due to an experiment. It can be justified from a decision-theoretic perspective [8, 15] as the expectation of a utility function based on Shannon information. The expected information gain enjoys other useful properties, such as invariance under reparameterization (inherited from the KL divergence). The EIG is also equivalent to the *mutual information* (MI) between  $X$  and  $Y|d$ , denoted  $\mathcal{I}(X; Y|d)$  [62]. We thus will use these two terms interchangeably. In the Bayesian linear-Gaussian model, maximizers of the expected information gain from prior to posterior coincide with Bayesian D-optimal designs, i.e.,  $d^* \in \arg \min_{d \in \Xi} \log \det \Sigma_{X|Y}(d)$ , where  $\Sigma_{X|Y}(d)$  is the design-dependent posterior covariance matrix. In general, however (e.g., outside of the linear-Gaussian setting), closed-form expressions for the EIG are unavailable. Estimating or bounding the EIG is in fact one of the *central challenges of nonlinear Bayesian experimental design*.

This paper proposes and analyzes new *transport-based estimation schemes for EIG in general nonlinear/non-Gaussian settings*. We address settings where the likelihood function and prior density can be evaluated directly, but also ‘‘implicit model’’ [17, 35] settings where one can only simulate (i.e., draw samples from) the prior and/or the data-generating distribution. To improve the estimation of EIG in high dimensions, we then introduce new *dimension reduction* schemes that seek low-dimensional projections of the data and parameters that best preserve the mutual information  $\mathcal{I}(X; Y)$ .

**1.1. Related work.** To frame our contributions, it is useful to expand the EIG (1.2) into expectations over marginal and conditional densities of  $X$  and  $Y$ . For notational simplicity, we drop explicit dependence on  $d$ :

$$(1.3) \quad \begin{aligned} \text{EIG} &= \int \int \pi_{X,Y}(x, y) \log \frac{\pi_{X,Y}(x, y)}{\pi_X(x)\pi_Y(y)} dx dy, \\ &= \mathbb{E}_{\pi_{X,Y}} \left[ \log \frac{\pi_{X|Y}(X|Y)}{\pi_X(X)} \right] \end{aligned}$$

$$(1.4) \quad = \mathbb{E}_{\pi_{X,Y}} \left[ \log \frac{\pi_{Y|X}(Y|X)}{\pi_Y(Y)} \right].$$

From the last two expressions, we see that estimating EIG requires either the *normalized* posterior density  $\pi_{X|Y}$  and the prior density  $\pi_X$  (1.3), or the conditional density  $\pi_{Y|X}$  (and hence the likelihood) and the evidence  $\pi_Y$  (1.4). To compute the outer expectation, all of these densities must be evaluated over a range of arguments  $x$  and  $y$ . Depending on what information is available, the problem of EIG estimation can be divided into settings of (roughly) increasing difficulty:

1. One can sample from the joint distribution of parameters and data  $\pi_{X,Y}$  (typically by drawing  $x^i \sim \pi_X$  and  $y^i \sim \pi_{Y|X}(\cdot|x^i)$ ) and also evaluate the prior density and likelihood function.
2. One can sample from joint distribution of parameters and data, but can only evaluate the marginal prior density  $\pi_X$ .
3. One can sample from the joint distribution of parameters and data, but cannot evaluate any of its marginal or conditional densities, and hence neither the prior density nor the likelihood.

The second and third settings above are “likelihood-free,” in that likelihood evaluations are unavailable and one can only simulate  $Y|X = x$  for any  $x$ . Data-generating models of this form are often called “implicit” and are the prototypical target of simulation-based inference methods [17]. The third setting is additionally “prior-free” and encompasses, for instance, generative prior models whose densities are unavailable. In both cases, the estimation of densities from samples is required.

In the first setting, a workhorse approach to EIG estimation has been nested Monte Carlo (NMC), which to our knowledge was first proposed by [56]. The core idea is to independently estimate the evidence  $\pi_Y(y)$  for different values of  $y$  and to embed these estimates in an outer Monte Carlo estimator of the expectation over  $Y$ , following (1.4). NMC is biased at finite sample sizes, but asymptotically unbiased; it also converges more slowly than standard Monte Carlo (see [54] and Section 4). For more details on NMC and its variants, we refer to [32, Section 3.1]. In the third setting, a classical method for estimating MI from samples is the nonparametric Kraskov–Stögbauer–Grassberger (KSG) estimator [37], which is based on the statistics of nearest-neighbor distances. The error of this estimator scales poorly with dimension [27], however, and it does not take advantage of smoothness in the associated densities.

A more modern family of sample-driven approaches involves constructing and optimizing variational bounds for EIG. In general, these approaches involve writing a variational representation of the mutual information and optimizing this representation (thus tightening the bound) over a family of so-called “critic” functions. Prominent examples include the ‘mutual information neural estimation’ approach of [7], which uses the Donsker–Varadhan variational representation of the KL divergence to construct a lower bound for MI, and then maximizes this bound over a family of critic functions represented by deep neural networks. Related methods include the “tractable unnormalized Barber–Agakov” bound introduced in [50] and the NWJ (Nguyen, Wainwright, Jordan) estimator of [45]. We refer to [50] for links among these and other variational bounds as well as trade-offs between the bias and variance of the resulting EIG estimators. One key point is that the optimal critic functions in these bounds typically coincide with the log-conditional density  $\log \pi_{Y|X}$ , the log-evidence  $\log \pi_Y$  and/or the log-density ratio  $\log \pi_{X|Y} - \log \pi_X = \log \pi_{Y|X} - \log \pi_Y$ , depending on the specifics of each construction.

The use of variational bounds is thus linked to density approximation, and an alternative approach is to optimize the deficit of a bound over families of density functions (i.e., non-negative functions that integrate to one) rather than generic critic functions. In the context of OED, this approach was first suggested by [26], who construct a lower bound for EIG by approximating the

posterior density  $\pi_{X|Y}$  and an upper bound for EIG by approximating the marginal  $\pi_Y$ . [26] demonstrate their approach using simple mean-field variational approximations in standard parametric families. Although such approximations are easy to implement, they do not, in general, yield tight bounds (e.g., if the true posterior or evidence is far from the chosen family). We also note that other estimators of EIG or mutual information are based on explicit density *ratio* estimation [53, 61, 9, 14]. In the machine learning literature, MI estimators that involve learning the density ratio are sometimes called ‘discriminative,’ while those based on learning the relevant densities directly are called ‘generative’ [40]. The comparative performance of these two classes of methods is in general not clear. Here, we will concentrate on the latter.

To this end, recent work has replaced the simpler density approximations of [26] with more flexible density approximations based on transportation of measure. For instance, [47, 23, 34] use conditional normalizing flows [55, 49] trained from samples of  $\pi_{X,Y}$  to approximate the density of  $\pi_{X|Y}$ . [36] instead constructs functional tensor-train approximations [18] of the triangular Knothe–Rosenblatt (KR) transport maps using direct evaluations of the joint density  $\pi_{X,Y}$ , which is further extended by [19] (combined with dimension reduction) to the sequential design setting. The approach we develop in this paper is also based on transport. In contrast with [36], we estimate the KR map from samples, and then use the associated plug-in estimator of any desired marginal and/or conditional density to form an EIG approximation. Depending on the problem setting, this approximation may also be an upper or lower bound. Our KR approximation is built on a general representation of monotone triangular maps that employs an invertible rectification operator, proposed in [5]; this operator transforms generic (non-monotone) functions  $f$  into monotone invertible functions, in particular triangular diffeomorphisms. The resulting EIG approximations are thus parameterized by  $f$ , and in this sense our EIG approximation comes full circle and is analogous to a critic-based variational bound. Crucially, under appropriate assumptions on the target distribution, we can take advantage of theory in [5] that guarantees recovery of the exact KR rearrangement and hence the exact marginals and conditionals. Thus, as the class of functions chosen to represent  $f$  is enriched, our bounds on the EIG can become arbitrarily tight. A specific version of EIG estimators explored in this paper was also demonstrated in [2].

The methods discussed above can be viewed effectively as *two-step procedures*: first, density approximations are learned from a set of “training samples”; then, the outer prior expectation (e.g., in (1.3) or (1.4)) is estimated via Monte Carlo with a separate set of “evaluation samples.” In many applications of OED, the generation of samples  $(y^i, x^i) \sim \pi_{Y,X}$  is the most computationally expensive element of the problem, as simulating the data  $Y|x^i$  requires evaluating a computationally intensive model. It is thus natural to ask how to make best use of a given sample budget—i.e., how to balance the training sample size  $N$  and evaluation sample size  $M$ , given a total sample size  $L = M + N$ , to minimize the mean squared error of the EIG estimate. To our knowledge, this sample allocation question has not yet been analyzed in the literature. Yet it is analogous to one that has previously been posed for NMC estimators, where the inner-loop sample size (for estimating the evidence  $\pi_Y(y)$  at any  $y$ ) must be balanced with the outer-loop sample size to achieve an optimal convergence rate of the MSE with  $L$  [6, 54].

We also note that most of the aforementioned EIG estimation methods, despite their widespread adoption, have only been applied in relatively low-dimensional regimes. Intuitively, these methods either explicitly or implicitly involve density estimation, and in the absence of further structure, the number of samples required for non-parametric or semi-parametric density estimation scales exponentially with dimension [43, 66]. Some papers on density ratio estimation do include high-dimensional examples, but these examples are either Gaussian [16] or the density ratio is parameterized by a simple exponential family [61]. Yet a recurring structure in high-dimensional Bayesian inference problems is that the change from prior to posterior is well-captured by a *low-dimensional*

*subspace* of the parameter space [20, 73, 11, 21, 19]. Similarly, conditioning on a *low-dimensional projection* of the realized observations  $y$  might closely approximate the result of conditioning on the full vector  $y$  [28, 33]. An information theoretic perspective on these projections is developed in [4]. In the present paper, we will use this perspective to create dimension reduction methods for OED, with *error guarantees* on the estimated value of the EIG.

Prior work on dimension reduction for OED has taken several forms. [70] uses Laplace approximations of the posterior, averaged over many realizations of the data, to approximate the EIG. These Laplace approximations are simplified using low-rank approximations of the prior-preconditioned Hessian of the log-likelihood, which is equivalent to parameter-space dimension reduction for linear (or linearized) problems [60]. [19] utilizes a likelihood-informed subspace to identify the informative direction, which is subsequently used to reduce the dimensionality of the parameters. Alternatively, in the setting of nonlinear inverse problems with additive noise, e.g.,  $Y = G(x) + \mathcal{E}$ , [71] constructs deep neural network approximations of the deterministic parameter-to-observable map  $G$  after performing dimension reduction in both the input space (of parameters  $X$ ) and output space (of observations  $Y$ ). The resulting surrogate is then used in an NMC estimator of the EIG. We employ the same parameter-space projection here, but a different projection of the observations that yields sharper error bounds. Moreover, instead of using NMC, we use both dimension reduction methods in transport-based EIG estimators.

**1.2. Contributions.** We summarize our main contributions as follows. We first present a general formulation for EIG estimation using transport-based density estimates. Our formulation is applicable to each of the three settings identified above, including implicit Bayesian models and goal-oriented variants of the OED problem. This formulation encompasses *any* method for transport-based marginal and conditional density estimation, including conditional normalizing flows [69] or conditional optimal transport [67], though we will demonstrate it here using an adaptive representation of monotone triangular maps that provides certain approximation guarantees [5].

As our first technical contribution, we analyze the underlying problem of sample allocation and convergence rates for such EIG estimators. Our results apply to any parametric density estimation scheme used within the EIG estimation framework. We develop an asymptotically optimal allocation of samples, between density estimation and the estimation of the outer expectation, to balance the decay rates of bias and variance and thus maximize the convergence rate of the mean squared error (MSE) of the EIG estimate. With this allocation, we show that this class of estimators converges at a *faster* rate than an optimally-balanced NMC scheme. We numerically verify the conditions yielding optimal rates, in a simple linear-Gaussian setting where the exact EIG is available analytically. As a demonstration, we then evaluate the performance and versatility of density-based EIG estimation algorithms for a non-Gaussian problem with various EIG objectives.

Our second technical contribution is to combine dimension reduction with transport-based EIG estimation to construct estimators of EIG in high dimensions. Our proposed dimension reduction scheme relies on minimizing an *upper bound* for the error in EIG induced by projecting both the parameters  $X$  and observations  $Y$  to lower-dimensional subspaces. The scheme for computing these projections originates in [4], where it was used for the purpose of posterior approximation, but this information theoretic perspective on dimension reduction is a natural fit for EIG in non-Gaussian settings. It seeks  $(r \ll n_x)$ -dimensional and  $(s \ll n_y)$ -dimensional projections  $X_r$  and  $Y_s$  of  $X$  and  $Y$ , respectively, that minimize an upper bound for the information loss  $\mathcal{I}(X; Y) - \mathcal{I}(X_r; Y_s)$  at any  $r$  and  $s$ . The preceding EIG estimation schemes can then be applied to the joint distribution of  $X_r$  and  $Y_s$ . We show that this dimension reduction approach outperforms other linear approaches, such as principal component analysis (PCA) and canonical correlation analysis (CCA). We also demonstrate how this scheme allows one to *trade off dimensionality with the modeling of non-*

*Gaussianity*: in many EIG estimation problems it is better to truncate the representation of the parameters and observations in a suitable basis and capture the non-Gaussianity of the resulting  $\pi_{X_r, Y_s}$ , than it is to make cruder (e.g., Gaussian) approximations of the full distribution  $\pi_{X, Y}$ .

The remainder of the paper is structured as follows. In Section 2, we first present a general formulation of transport-based EIG estimation, where block-triangular transport maps are used to approximate the relevant marginal and/or conditional densities in Bayesian problem settings ranging from standard to simulation-based. We also show how maximum likelihood estimation of block-triangular transport maps corresponds to tightening the bounds on EIG in certain cases. In Section 2.3, we present our results on optimal sample allocations and convergence rates. In Section 3, we describe the construction of parameter-space and observation-space projections that minimize the loss of mutual information, and show how these projections are applied to the estimation of EIG in high dimensions. Section 4 contains our numerical experiments, where we verify our results on optimal sample allocation using a linear Gaussian example, demonstrate EIG estimation in non-Gaussian settings, and explore the impact of dimension reduction and density approximations on EIG estimates in a high-dimensional PDE-constrained Bayesian inverse problem.

**2. EIG estimation using transportation of measure.** In this section, we first formulate upper and lower bounds for EIG based on density approximations in Subsection 2.1. Second, we show how transport-based density estimates can be used to realize these bounds and elucidate the link between maximum likelihood estimation and tightness of the bounds in Subsection 2.2. Lastly, we analyze the asymptotic convergence rate of this class of EIG estimators and derive an asymptotically-optimal rule for allocating samples between density estimation and the estimation of an outer prior expectation in Subsection 2.3.

**2.1. EIG bounds and estimators.** Recall the expressions (1.3) and (1.4) for the EIG from prior to posterior: the first involves the normalized posterior density  $\pi_{X|Y}$  and the second involves the evidence  $\pi_Y$ . In most settings, neither of these densities can be evaluated exactly. Instead we can only evaluate approximations, denoted by  $\tilde{\pi}_{X|Y}$  and  $\tilde{\pi}_Y$ , respectively. Any such approximating densities yield lower and upper bounds, respectively, for the EIG:

$$\begin{aligned}
 \mathbb{E}_{\pi_{X, Y}} \left[ \log \frac{\tilde{\pi}_{X|Y}(X|Y)}{\pi_X(X)} \right] &\leq \mathbb{E}_{\pi_Y} \left[ \mathcal{D}_{\text{KL}}(\pi_{X|Y} || \tilde{\pi}_{X|Y}) \right] + \mathbb{E}_{\pi_{X, Y}} \left[ \log \frac{\tilde{\pi}_{X|Y}(X|Y)}{\pi_X(X)} \right] \\
 &= \text{EIG} \\
 (2.1) \quad &= \mathbb{E}_{\pi_{X, Y}} \left[ \log \frac{\pi_{Y|X}(Y|X)}{\tilde{\pi}_Y(Y)} \right] - \mathcal{D}_{\text{KL}}(\pi_Y || \tilde{\pi}_Y) \leq \mathbb{E}_{\pi_{X, Y}} \left[ \log \frac{\pi_{Y|X}(Y|X)}{\tilde{\pi}_Y(Y)} \right]
 \end{aligned}$$

We refer readers to [26, 50] for the derivation. We note that equality holds in (2.1) if and only if the relevant approximation is exact, i.e., if  $\tilde{\pi}_{X|Y} = \pi_{X|Y}$  or if  $\tilde{\pi}_Y = \pi_Y$ , and that the deficits in the inequalities are precisely  $\mathbb{E}_{\pi_Y} \left[ \mathcal{D}_{\text{KL}}(\pi_{X|Y} || \tilde{\pi}_{X|Y}) \right]$  and  $\mathcal{D}_{\text{KL}}(\pi_Y || \tilde{\pi}_Y)$ . Therefore, approximating the EIG by maximizing the lower bound or minimizing the upper bound is equivalent to finding good approximations in this Kullback–Leibler sense. Given the appropriate density approximations and  $M$  i.i.d. joint samples  $\{x^i, y^i\}_{i=1}^M \sim \pi_{X, Y}$ , we can also construct Monte Carlo estimators of the lower or upper bounds that satisfy the inequalities in (2.1) with high probability; we will define such estimators explicitly below.

If we replace the prior or likelihood in equations (1.3) or (1.4) with approximations  $\tilde{\pi}_X$  and  $\tilde{\pi}_{Y|X}$ , the expected information gain (EIG) is neither upper-bounded nor lower-bounded [26]. Specifically, neither  $\mathbb{E}_{\pi_{X, Y}} \left[ \log \frac{\tilde{\pi}_{X|Y}(x|y)}{\tilde{\pi}_X(x)} \right]$  nor  $\mathbb{E}_{\pi_{X, Y}} \left[ \log \frac{\tilde{\pi}_{Y|X}(y|x)}{\tilde{\pi}_Y(y)} \right]$  serves as a bound for EIG. Furthermore, in

cases where both the prior *and* likelihood are intractable, it becomes necessary to approximate both the numerator and denominator densities. This requires using Monte Carlo estimators for  $\mathbb{E}_{\pi_{X,Y}} \left[ \log \frac{\tilde{\pi}_{X|Y}(x|y)}{\tilde{\pi}_X(x)} \right]$  and  $\mathbb{E}_{\pi_{X,Y}} \left[ \log \frac{\tilde{\pi}_{Y|X}(y|x)}{\tilde{\pi}_Y(y)} \right]$ . While these estimators can be consistent, they do not provide (stochastic) bounds for EIG.

To summarize, evaluating EIG according to the expressions above involves: (i) approximating a conditional and/or a marginal density, depending on what problem information is *a priori* available (e.g., samples versus the ability to evaluate exact densities); and (ii) using samples  $\{x^i, y^i\}_{i=1}^M$  from  $\pi_{X,Y}$  to approximate the outer expectation. We then have four estimators that are useful in practice:

$$(2.2) \quad \widetilde{\text{EIG}}_{\text{m}} := \frac{1}{M} \sum_{i=1}^M \log \frac{\pi_{Y|X}(y^i|x^i)}{\tilde{\pi}_Y(y^i)},$$

$$(2.3) \quad \widetilde{\text{EIG}}_{\text{pos}} := \frac{1}{M} \sum_{i=1}^M \log \frac{\tilde{\pi}_{X|Y}(x^i|y^i)}{\pi_X(x^i)},$$

$$(2.4) \quad \widetilde{\text{EIG}}_{\text{lik}} := \frac{1}{M} \sum_{i=1}^M \log \frac{\tilde{\pi}_{Y|X}(y^i|x^i)}{\tilde{\pi}_Y(y^i)},$$

$$(2.5) \quad \widetilde{\text{EIG}}_{\text{pr}} := \frac{1}{M} \sum_{i=1}^M \log \frac{\tilde{\pi}_{X|Y}(x^i|y^i)}{\tilde{\pi}_X(x^i)}.$$

The first two provide stochastic upper and lower bounds as described in (2.1). The last three can be used in the likelihood-free setting, as the expressions do not involve evaluating the likelihood function  $\pi_{Y|X}$ ; the second does require evaluating the prior density, however. In the next section, we will introduce an approach to compute these four EIG estimators using transport maps.

**2.2. Transport maps for density estimation.** Measure transport provides an expressive and infinitely refinable way of approximating complex probability densities. Here we give a brief and intuitive introduction to this approach; for more details, we refer the reader to [42, 59, 5]. To illustrate key ideas, we first set aside the OED problem and the specific probability distributions it entails, returning to them in Section 2.2.3.

Let  $\pi$  denote an intractable target distribution that we would like to characterize, and let  $\eta$  denote a reference distribution whose density we can easily evaluate—for example, a standard Gaussian. We would like to find a map  $S: \mathbb{R}^n \rightarrow \mathbb{R}^n$  such that  $\eta(A) = \pi(S^{-1}(A))$  for any measurable set  $A$ . A map that satisfies this property is said to *push forward*  $\pi$  to  $\eta$ , or equivalently to *pull back*  $\eta$  to  $\pi$ . The existence of  $S$  is guaranteed when both  $\pi$  and  $\eta$  are absolutely continuous with respect to Lebesgue measure [57]. We use subscript and superscript  $\sharp$  symbols to denote the pushforward and pullback operations, respectively:

$$\begin{aligned} S_{\sharp} \pi &= \eta \\ S^{\sharp} \eta &= \pi. \end{aligned}$$

When  $S$  is invertible and sufficiently smooth, we can write the target density  $\pi$  explicitly in terms of the reference density using the change-of-variables formula<sup>2</sup>

$$(2.6) \quad \pi(z) = S^{\sharp} \eta(z) = \eta \circ S(z) |\det \nabla S(z)|.$$

---

<sup>2</sup>Here, since all probability measures are assumed to have Lebesgue densities, we abuse notation by using the same symbol to denote either object.

This expression lets us estimate the density  $\pi$  simply by plugging in an estimate for the map  $S$  [66]. Moreover, the map allows us to sample from the target distribution by evaluating the inverse map  $S^{-1}(z^i)$  at reference samples  $z^i \sim \eta$ .

For absolutely continuous measures  $\eta$  and  $\pi$ , there are infinitely many transport maps coupling one to the other. For the purpose of EIG estimation, we are particularly interested in marginal and conditional density estimation. A triangular transport map, known as the Knothe–Rosenblatt (KR) rearrangement [64, 57, 10], is particularly well suited to this goal. The KR rearrangement is the unique<sup>3</sup> map  $S$  satisfying  $S\# \pi = \eta$  that has the *lower-triangular* structure

$$(2.7) \quad S(z) = \begin{bmatrix} S^1(z_1) \\ S^2(z_1, z_2) \\ \vdots \\ S^n(z_1, z_2, \dots, z_n) \end{bmatrix},$$

and where each component function  $S^k : \mathbb{R}^k \rightarrow \mathbb{R}$  is monotone in its last argument, i.e.,  $z_k \mapsto S^k(z_1, \dots, z_k)$  is monotone (increasing) for all  $(z_1, \dots, z_{k-1}) \in \mathbb{R}^{k-1}$ ,  $k = 1, \dots, n$ . Component functions of the triangular map correspond to conditionals of  $\pi$  [57], and thus this map immediately provides conditional density estimates using an adaptation of (2.6), which we will detail below. Strict monotonicity guarantees that the map  $S$  is invertible, and evaluations of the inverse map  $S^{-1}$  essentially involve a sequence of  $n$  univariate root-finding problems. Moreover, the Jacobian determinant of  $S$  is easy to evaluate as  $\det \nabla S(z) = \prod_{k=1}^n \partial_k S^k(z_{1:k})$ .

Although we have the freedom to choose  $\eta$  to be any distribution on  $\mathbb{R}^n$ , putting  $\eta$  equal to the standard normal distribution  $\mathcal{N}(0, I_n)$  substantially simplifies the problem of estimating the map  $S$ , which we discuss next.

**2.2.1. Maximum likelihood estimation of transport maps.** Here we formulate an optimization method for identifying lower triangular transport maps  $S$ , given a set of samples drawn from  $\pi$ . One approach is to minimize the KL divergence from  $S\#\eta$  to  $\pi$  over a class of monotone triangular functions  $\mathcal{S}$  [42], i.e.,

$$(2.8) \quad S_{\text{OPT}} = \arg \min_{S \in \mathcal{S}} \mathcal{D}_{\text{KL}}(\pi || S\#\eta).$$

Choosing  $\eta$  to be the standard Gaussian distribution, we can then write the objective in (2.8) as

$$\begin{aligned} \mathcal{D}_{\text{KL}}(\pi || S\#\eta) &= \mathbb{E}_{z \sim \pi} \left[ \log \frac{\pi(z)}{S\#\eta(z)} \right] \\ &= \mathbb{E}_{z \sim \pi} [\log \pi] + \frac{n}{2} \log(2\pi) + \sum_{k=1}^n \mathbb{E}_{z \sim \pi} \left[ \frac{1}{2} S^k(z_{1:k})^2 - \log \partial_k S^k(z_{1:k}) \right]. \end{aligned}$$

Since the first two terms are independent of  $S$ , and each term in the summation depends only on  $S^k$ , the optimization problem is separable; we can learn each map component independently by minimizing the objective

$$(2.9) \quad J_k(S^k) := \mathbb{E}_{z \sim \pi} \left[ \frac{1}{2} S^k(z_{1:k})^2 - \log \partial_k S^k(z_{1:k}) \right],$$

---

<sup>3</sup>Up to re-labeling/re-ordering of the coordinates.

for  $k = 1, \dots, n$ . Note that  $J_k(S^k)$  is convex in  $S^k$  for every  $k$ . Therefore the optimization problem (2.8), subject to the linear constraints  $\partial_k S^k(z_{1:k}) > 0$  for  $k = 1, \dots, n$ , is a convex problem. In practice, we replace the expectation in (2.9) with its empirical approximation,

$$(2.10) \quad \widehat{J}_k(S) = \frac{1}{N} \sum_{i=1}^N \left[ \frac{1}{2} S(z_{1:k}^i)^2 - \log \partial_k S(z_{1:k}^i) \right],$$

where  $\{z_{1:k}^i\}_{i=1}^N$  are i.i.d. samples from  $\pi$ . Let  $\widehat{S}_{\text{OPT}}^k = \arg \min_{S^k \in \mathcal{S}^k} \widehat{J}_k(S^k)$ , where  $\mathcal{S}^k$  is a space of maps from  $\mathbb{R}^k$  to  $\mathbb{R}$  satisfying the monotonicity constraint  $\partial_k S^k > 0$ . As explained in [5, 66], each  $\widehat{S}_{\text{OPT}}^k$  is a *maximum likelihood* estimate of the corresponding map component  $S^k$ , and concatenating these functions yields a maximum likelihood estimate of the entire triangular map:  $\widehat{S}_{\text{OPT}} = (\widehat{S}_{\text{OPT}}^1, \widehat{S}_{\text{OPT}}^2, \dots, \widehat{S}_{\text{OPT}}^n)$ .

We can then form a plug-in estimate of the density  $\pi$ :  $\widehat{\pi}(z) := \widehat{S}_{\text{OPT}}^\# \eta(z)$ . Thus  $\widehat{\pi}$  is a transport-induced estimate of the target density, given  $N$  samples.

**2.2.2. Parameterization and the choice of basis functions.** Solving the maximum likelihood estimation problem above requires parameterizing classes of monotone maps; specifically, we must explicitly construct classes  $\mathcal{S}^k$  of map components  $S^k: \mathbb{R}^k \rightarrow \mathbb{R}$  that are strictly increasing in their last argument, i.e., satisfying  $\partial_k S^k(x_{1:k}) > 0$ ,  $\forall x_{1:k} \in \mathbb{R}^k$ . Here we do so by expressing  $S^k$  as the transformation of an arbitrary (non-monotone) function  $f: \mathbb{R}^k \rightarrow \mathbb{R}$  through the operator  $\mathcal{R}_k$ :

$$(2.11) \quad S^k(z_{1:k}) = \mathcal{R}_k(f)(z_{1:k}) := f(z_{1:k-1}, 0) + \int_0^{z_k} g(\partial_k f(z_{1:k-1}, t)) dt,$$

where  $g: \mathbb{R} \rightarrow \mathbb{R}_{>0}$  is strictly positive and bijective, and satisfies further regularity conditions detailed in [5]. We substitute this representation of each  $S^k$  into (2.10) and solve the resulting *unconstrained* minimization problem,  $\min_f \widehat{J}_k(\mathcal{R}_k(f))$  over some linear space of functions  $\mathcal{V}_k \ni f$ . As explained in [5], this construction provides important optimization guarantees: there are no spurious local minima (every local minimizer  $f^*$  is global minimizer) and under certain tail conditions on  $\pi$  and  $f$ , we provably recover the true KR rearrangement.

Here, we parameterize  $f$  using a linear expansion of tensor-product Hermite polynomials  $\psi_\alpha$  as  $f(z_{1:k}) = \sum_\alpha c_\alpha \psi_\alpha(z_{1:k})$  and solve for its coefficients  $c_\alpha$ . We refine this polynomial space using a greedy adaptive procedure and apply cross-validation to select the total number of polynomial basis functions to retain. We refer to [5] for complete details on these numerical procedures.

We note also that while our focus thus far in Section 2.2 and Subsection 2.2.2, and in the numerical experiments reported later in this paper, is on *strictly* triangular maps, we will see in Section 2.2.3 that *block triangular* maps as described in [3] are also suitable for estimating the marginal and conditional densities relevant to the OED problem. In contrast with the strictly triangular case, there is no unique choice of block-triangular map. One natural choice is a conditional Brenier map, as described in [12, 3, 67]. Another broad family of choices are given by conditional normalizing flows, which are specific parameterizations of the bottom block of a block-triangular map. We use strictly triangular maps in our numerical experiments because the associated computations are relatively fast, and because they enjoy the optimization guarantees mentioned above; to our knowledge, such guarantees are not available for other continuous map representations.

**2.2.3. From marginal and conditional density estimation to EIG bounds.** In the previous discussion, we let  $z$  be a generic vector in  $\mathbb{R}^n$ . Now let  $z = (y, x)$  where  $x \in \mathbb{R}^{n_x}$  and  $y \in \mathbb{R}^{n_y}$ . Given samples from the joint distribution  $\pi_{X,Y}$ , we consider the problem of estimating the densities  $\pi_Y$  and  $\pi_{X|Y}$ . To do so, we construct a *block lower-triangular* map  $S: \mathbb{R}^{n_y+n_x} \rightarrow \mathbb{R}^{n_y+n_x}$  of the

form:

$$S(y, x) = \begin{bmatrix} S^{\mathcal{Y}}(y) \\ S^{\mathcal{X}}(y, x) \end{bmatrix},$$

where  $S^{\mathcal{Y}}: \mathbb{R}^{n_y} \rightarrow \mathbb{R}^{n_y}$  and  $S^{\mathcal{X}}: \mathbb{R}^{n_y+n_x} \rightarrow \mathbb{R}^{n_x}$ . We choose  $\eta$  to be standard Gaussian on  $\mathbb{R}^{n_y+n_x}$ . Our parameterizations ensure that  $S^{\mathcal{Y}}$  is invertible and that  $\nabla_y S^{\mathcal{Y}}$  exists, and similarly that  $x \mapsto S^{\mathcal{X}}(y, x)$  is invertible and that  $\nabla_x S^{\mathcal{X}}(y, x)$  exists for every  $y \in \mathbb{R}^{n_y}$ ; this applies specifically to the numerical representations of triangular maps mentioned above. Note that such properties are satisfied almost everywhere by the KR map for absolutely continuous distributions with full support; see [59, Sec. 3] and [57, Sec. 2.3] for a discussion.

If we select our reference distribution  $\eta$  to be *any* distribution whose density factorizes as  $\eta(x, y) = \eta_X(x)\eta_Y(y)$  (which clearly includes the standard normal), [3, Theorem 2.4] shows that we can express the marginal density of  $Y$  as  $\pi_Y = (S^{\mathcal{Y}})^{\#}\eta_Y$  and the posterior density of  $X$  as  $\pi_{X|Y=y} = S^{\mathcal{X}}(y, \cdot)^{\#}\eta_X$  for any  $y \in \mathbb{R}^{n_y}$ .

By reversing the ordering of  $x$  and  $y$ , we obtain another lower-triangular map

$$U(x, y) = \begin{bmatrix} U^{\mathcal{X}}(x) \\ U^{\mathcal{Y}}(x, y) \end{bmatrix}.$$

We can then exchange the roles of  $y$  and  $x$  and repeat the procedure above to approximate the prior  $\pi_X$  and the likelihood  $\pi_{Y|X}$ . Thus, the two maps with both variable orderings provide all four density estimates,  $\hat{\pi}_X$ ,  $\hat{\pi}_{X|Y}$ ,  $\hat{\pi}_Y$ , and  $\hat{\pi}_{Y|X}$ , as follows:

$$\begin{aligned} \hat{\pi}_X &= (\hat{U}^{\mathcal{X}})^{\#}\eta_X, \\ \hat{\pi}_{X|Y=y} &= (\hat{S}^{\mathcal{X}}(y, \cdot))^{\#}\eta_X, \\ \hat{\pi}_Y &= (\hat{S}^{\mathcal{Y}})^{\#}\eta_Y, \\ \hat{\pi}_{Y|X=x} &= (\hat{U}^{\mathcal{Y}}(x, \cdot))^{\#}\eta_Y. \end{aligned}$$

where we use  $\hat{S}$  and  $\hat{U}$  to denote maximum likelihood estimates of  $S$  and  $U$ . These density estimates can then be substituted into any of (2.2)–(2.5). We summarize the proposed EIG estimation scheme in Algorithm 2.1.

---

**Algorithm 2.1** EIG estimation using transport maps

---

- 1: **Input:** Partition the i.i.d. pairs of joint samples  $\{(x^i, y^i)\}_{i=1}^L \sim \pi_{X,Y}$  into  $N$  training and  $M$  evaluation samples, such that  $L = N + M$
  - 2: **Output:** EIG estimator
  - 3: Use  $N$  training samples to learn the transport maps  $\hat{S}$  and/or  $\hat{U}$ , and form plug-in estimates of densities that are not available in closed form, e.g.,  $\hat{\pi}_Y$ ,  $\hat{\pi}_{Y|X}$ ,  $\hat{\pi}_X$ , and/or  $\hat{\pi}_{X|Y}$ .
  - 4: Use  $M$  pairs of samples to estimate EIG by evaluating the empirical averages  $\frac{1}{M} \sum_{i=1}^M \log \frac{\pi_{Y|X}(y^i|x^i)}{\hat{\pi}_Y(y^i)}$ ,  $\frac{1}{M} \sum_{i=1}^M \log \frac{\hat{\pi}_{X|Y}(x^i|y^i)}{\pi_X(x^i)}$ ,  $\frac{1}{M} \sum_{i=1}^M \log \frac{\hat{\pi}_{Y|X}(y^i|x^i)}{\hat{\pi}_Y(y^i)}$ , and/or  $\frac{1}{M} \sum_{i=1}^M \log \frac{\hat{\pi}_{X|Y}(x^i|y^i)}{\hat{\pi}_X(x^i)}$ .
- 

Now we make the crucial observation that solving the optimization problem (2.8) is equivalent to tightening the bounds in (2.1). Observe that the objective of (2.8) separates:

$$\mathcal{D}_{\text{KL}}(\pi_{Y,X} \| S^{\#}\eta_{Y,X}) = \mathbb{E}_{\pi_{Y,X}} \left[ \log \frac{\pi_{Y,X}(Y, X)}{(S^{\#}\eta_{Y,X})(Y, X)} \right]$$

$$\begin{aligned}
&= \mathbb{E}_{\pi_Y} \left[ \log \frac{\pi_Y(Y)}{(S^{\mathcal{Y}, \#} \eta_Y)(Y)} \right] + \mathbb{E}_{\pi_{Y,X}} \left[ \log \frac{\pi_{X|Y}(X|Y)}{(S^{\mathcal{X}}(Y, \cdot)^{\#} \eta_X)(X)} \right] \\
&= \mathcal{D}_{\text{KL}} \left( \pi_Y \| S^{\mathcal{Y}, \#} \eta_Y \right) + \mathbb{E}_{\pi_Y} \left[ \mathcal{D}_{\text{KL}} \left( \pi_{X|Y} \| S^{\mathcal{X}}(y, \cdot)^{\#} \eta_X \right) \right],
\end{aligned}$$

Therefore, finding  $\arg \min_{S \in \mathcal{S}} \mathcal{D}_{\text{KL}} \left( \pi_{Y,X} \| S^{\#} \eta_{Y,X} \right)$  is equivalent to solving both

$$\min_{S^{\mathcal{X}} \in \mathcal{S}^{\mathcal{X}}} \mathbb{E}_{\pi_Y} \left[ \mathcal{D}_{\text{KL}} \left( \pi_{X|Y} \| S^{\mathcal{X}}(y, \cdot)^{\#} \eta_X \right) \right] \quad \text{and} \quad \min_{S^{\mathcal{Y}} \in \mathcal{S}^{\mathcal{Y}}} \mathcal{D}_{\text{KL}} \left( \pi_Y \| S^{\mathcal{Y}, \#} \eta_Y \right),$$

where  $\mathcal{S} = \mathcal{S}^{\mathcal{Y}} \times \mathcal{S}^{\mathcal{X}}$ . As noted in [Subsection 2.1](#), these two terms are *precisely* the deficits of the upper and lower bounds in [\(2.1\)](#). Therefore, given a particular parameterization of the transport map, minimizing these two quantities is equivalent to maximizing and minimizing, respectively, the lower and upper bounds in [\(2.1\)](#). Maximum likelihood estimation of the maps  $S^{\mathcal{X}}$  and  $S^{\mathcal{Y}}$  is a sample approximation of these bound-tightening problems.

**2.3. Convergence analysis and optimal sample allocation.** Given that the transport maps are estimated using  $N$  training samples (see [\(2.10\)](#)), and the empirical average is computed using  $M$  evaluation samples (see [\(2.2\)](#), [\(2.3\)](#), [\(2.4\)](#), [\(2.5\)](#)), we aim to investigate the optimal sample allocation between the number of training samples  $N$  and the number of evaluation samples  $M$ , given a total of  $L = N + M$  samples, with the objective of minimizing the MSE of the EIG estimator. Here, we use  $\widehat{\text{EIG}}_{M,N}$  to indicate that the EIG estimator is obtained using  $N$  training samples and  $M$  evaluation samples. For an EIG estimator  $\widehat{\text{EIG}}_{M,N}$ , the bias is defined as

$$\text{bias} = \mathbb{E} \left[ \widehat{\text{EIG}}_{M,N} - \text{EIG} \right],$$

where the expectation is taken over all the non-deterministic terms: the random map obtained through  $N$  training samples and Monte Carlo sum calculated using  $M$  evaluation samples. We denote the variance of the EIG estimator by

$$\text{variance} = \mathbb{V} \left[ \widehat{\text{EIG}}_{M,N} \right].$$

Recall that the MSE is defined as

$$\text{MSE} = \text{bias}^2 + \text{variance}.$$

Now consider the transport map  $S$  parameterized by coefficients  $\alpha \in \mathbb{R}^p$ , with  $\alpha^*$  being the optimizer that minimizes the exact KL divergence. That is,

$$\alpha^* = \arg \min_{\alpha} \mathcal{D}_{\text{KL}} \left( \pi \| S_{\alpha}^{\#} \eta \right) = \arg \max_{\alpha} \mathbb{E}_{\pi} \left[ \log S_{\alpha}^{\#} \eta(z) \right],$$

where  $\pi$  is a generic probability measure.

To simplify the exposition, we first consider estimating only the marginal distribution  $\pi_Y$ . Let  $\pi_Y(y)$  denote the true density evaluated at  $y$ . Let

$$(2.12) \quad \mathcal{Q}^{\mathcal{Y}} = \{q_Y(\cdot; \alpha) : \alpha \in \mathbb{R}^p\}$$

be a parametric class of densities within which we will approximate  $\pi_Y$ . For example, in the specific case of the transport-based approximations, an element  $q_Y \in \mathcal{Q}^{\mathcal{Y}}$  can be written as the pullback of

$\eta_Y$  by  $S_\alpha^\mathcal{Y}$ , i.e.,  $(S_\alpha^\mathcal{Y} \eta_Y)(y) = q_Y(y; \alpha)$ , where  $S_\alpha^\mathcal{Y}$  belongs to the parametric class of transport maps  $\mathcal{S} = \{S_\alpha : \alpha \in \mathbb{R}^p\}$  and  $\eta_Y$  is the standard normal. The results below, however, apply to any class of densities parameterized by  $\alpha$ .

Given i.i.d. samples  $\{y^i\}_{i=1}^N \sim \pi_Y$ , the maximum likelihood estimator (MLE) of  $\alpha$  follows from simply replacing the expectation in (2.3) by its empirical approximation,

$$\hat{\alpha}_N = \arg \max_{\alpha} \frac{1}{N} \sum_{i=1}^N \log q_Y(y^i; \alpha),$$

where the subscript  $N$  indicates that  $\hat{\alpha}_N$  is learned using  $N$  training samples.

**Assumption 2.1.** The target density  $\pi_Y$  is in-class for the parametric model, i.e., there exists a parameter  $\alpha^*$  such that  $q_Y(y; \alpha^*) = \pi_Y(y)$ .

**Assumption 2.2.** The maximum likelihood estimator  $\hat{\alpha}_N$  is consistent and asymptotically normal. That is  $\hat{\alpha}_N$  converges to  $\alpha^*$  in probability as  $N \rightarrow \infty$  and  $\sqrt{N}(\hat{\alpha}_N - \alpha^*)$  converges to  $\mathcal{N}(0, I(\alpha^*)^{-1})$  in distribution, where the entries of  $I(\alpha)$  are defined as

$$(2.13) \quad I(\alpha)_{ij} = -\mathbb{E}_{\pi_Y} \left[ \partial_{\alpha_i} \partial_{\alpha_j} \log q_Y(y; \alpha) \right].$$

We refer the reader to Section 10.6.2 of [13] for the regularity conditions that guarantee the consistency and asymptotic normality of the MLE. We now present our main result on the bias and variance of an resulting EIG estimator constructed using an approximate density based on transport maps.

**Theorem 2.3.** Under the Assumptions 2.1 and 2.2, let  $g(\alpha) = \mathbb{E}_{\pi_Y} [\log q_Y(y; \alpha)]$ , where  $q_Y \in \mathcal{Q}^\mathcal{Y}$ . Suppose  $g$  is continuous and bounded, and that both  $\nabla g(\alpha)$ ,  $\nabla^2 g(\alpha)$  exist and are continuous. Then, the EIG estimator

$$\frac{1}{M} \sum_{i=1}^M \log \frac{\pi_{Y|X}(y^i|x^i)}{q_Y(y^i; \hat{\alpha}_N)},$$

has bias converging to zero at a rate of  $O(1/N)$  and variance converging to zero at a rate of  $O(1/M + 1/N^2)$ . Thus, the MSE converges at a rate of  $O(1/M + 1/N^2)$ .

The proof of Theorem 2.3 is presented in Appendix 1. We then define  $\mathcal{Q}^{\mathcal{Y}|X}$  as

$$\mathcal{Q}^{\mathcal{Y}|X} = \{q_{Y|X}(\cdot|x; \beta) : \beta \in \mathbb{R}^t\}.$$

Here,  $\beta$  denotes the coefficients for parametrizing the likelihood function. In our case,  $q_{Y|X} \in \mathcal{Q}^{\mathcal{Y}|X}$ , where  $q_{Y|X}(y|x; \beta)$  denote the pullback of  $\eta_Y$  by  $U_\beta^\mathcal{Y}(x, \cdot)$ . That is,  $q_{Y|X}(y|x; \beta) = \left( U_\beta^\mathcal{Y}(x, \cdot) \# \eta_Y \right)(y)$ , and  $U_\beta^\mathcal{Y}(x, \cdot)$  is an element in the parametric class  $\mathcal{U} = \{U_\beta(x, \cdot) : \beta \in \mathbb{R}^t\}$ . Similar to Assumptions 2.1 and 2.2, we list the following two assumptions for  $q_{Y|X}$ .

**Assumption 2.4.** The target density  $\pi_{Y|X}$  is in-class for the parametric model, i.e., there exists a parameter  $\beta^*$  such that  $q_{Y|X}(y|x; \beta^*) = \pi_{Y|X}(y|x)$ .

Let  $\hat{\beta}_N$  be the MLE for  $\beta$ ,

$$\hat{\beta}_N = \arg \max_{\beta} \frac{1}{N} \sum_{i=1}^N \log q_{Y|X}(y^i|x^i; \beta).$$

*Assumption 2.5.* The maximum likelihood estimator  $\widehat{\beta}_N$  is consistent and asymptotically normal.

**Theorem 2.6.** *Under the Assumptions 2.4 and 2.5, let  $h(\beta) = \mathbb{E}_{\pi_{X,Y}} \left[ \log q_{Y|X}(y|x; \beta) \right]$ , where  $q_{Y|X} \in \mathcal{Q}^{\mathcal{Y}|\mathcal{X}}$ . Suppose  $h$  is continuous and bounded, and that both  $\nabla h(\beta), \nabla^2 h(\beta)$  exist and are continuous. Then, the EIG estimator  $\frac{1}{M} \sum_{i=1}^M \log \frac{q_{Y|X}(y^i|x^i; \widehat{\beta}_N)}{\pi_Y(y^i)}$  has bias converging to zero at a rate of  $O(1/N)$  and variance converging to zero at a rate of  $O(1/M + 1/N^2)$ . Thus, the MSE converges at a rate of  $O(1/M + 1/N^2)$ .*

**Theorem 2.7.** *Under the Assumptions 2.1, 2.2, 2.4 and 2.5, suppose  $g$  and  $h$  are both continuous and bounded, and that  $\nabla g(\alpha), \nabla^2 g(\alpha)$  and  $\nabla h(\beta), \nabla^2 h(\beta)$  exist and are continuous in some neighborhood of  $\alpha^*$  and  $\beta^*$ , respectively. Then bias of the EIG estimator*

$$\frac{1}{M} \sum_{i=1}^M \log \frac{q_{Y|X}(y^i|x^i; \widehat{\beta}_N)}{q_Y(y^i; \widehat{\alpha}_N)},$$

where  $\{x^i, y^i\}_{i=1}^{L=N+M} \sim \pi_{X,Y}$ , converges at a rate of  $O(1/N)$ , and the variance converges at a rate of  $O(1/M + 1/N^2)$ . Therefore, the MSE converges at a rate of  $O(1/M + 1/N^2)$ .

The proof is deferred to Appendix 1. After analyzing the convergence rate, we can then explore the optimal sample allocation between the training and evaluation samples.

**Corollary 2.8.** *In the context of Theorem 2.3 and Theorem 2.7, given  $L$  samples from the joint distribution  $\pi_{X,Y}$ , the optimal allocation between the training and evaluation samples should be set as  $\frac{M}{N} \sim O(L^{1/3})$ . Correspondingly, the optimal convergence rate of the MSE is  $O(L^{-1})$ .*

The proof of this corollary is provided in Appendix 4. We observe that if  $\frac{M}{N} \sim O(L^p)$  for some  $p > 0$ , the mean squared error (MSE) decreases at a rate of  $2L^{p-2} + L^{-p-1} + L^{2p-2} + L^{-2} + L^{-1}$ . If  $p > 1/2$ , the leading term has an order greater than  $-1$ . For all  $p \in (0, \frac{1}{2}]$ , the asymptotic convergence rate remains  $O(L^{-1})$ . The optimal value,  $p = 1/3$ , is obtained by solving a root-finding problem (see Appendix 4 for more detail), where the difference lies in the order of the non-leading term. The rate of convergence is confirmed in the numerical examples presented in Subsection 4.1.

**3. EIG estimation in high dimensions.** When the dimension of the parameters and data is high, directly estimating MI becomes computationally expensive. To address this, we aim to reduce the dimensionality of the parameters and data simultaneously, ensuring that the lower-dimensional subspace still preserves the mutual information. In this section, we apply the dimension reduction methods proposed in [4]. Given two unitary matrices  $U = [U_r, U_\perp] \in \mathbb{R}^{n_x \times n_x}$  and  $V = [V_s, V_\perp] \in \mathbb{R}^{n_y \times n_y}$ , consider the decompositions

$$\begin{aligned} X &= U_r X_r + U_\perp X_\perp, \quad \text{where } X_r = U_r^\top X, X_\perp = U_\perp^\top X \\ Y &= V_s Y_s + V_\perp Y_\perp, \quad \text{where } Y_s = V_s^\top Y, Y_\perp = V_\perp^\top Y. \end{aligned}$$

We interpret  $X_\perp$  as the non-informed part of  $X$ , and similarly  $Y_\perp$  is interpreted as the non-informative part of  $Y$ . Given such a decomposition, we define approximate posterior  $\pi_{X|Y}^*$  as  $\pi_{X|Y}^*(x|y) := \pi_{X_r|Y_s}(x_r|y_s) \pi_{X_\perp|X_r}(x_\perp|x_r)$ . While this approximation is equal to the true posterior under the conditional independence conditions  $X_\perp \perp\!\!\!\perp Y \mid X_r$  and  $X_r \perp\!\!\!\perp Y_\perp \mid Y_s$ , these conditions are difficult to satisfy in practice, which generally leads to  $\pi_{X|Y}^* \neq \pi_{X|Y}$ . Therefore, we aim to find transformations  $U$  and  $V$  such that the expected KL divergence from the approximate posterior

$\pi_{X|Y}^*$  to the true posterior  $\pi_{X|Y}$  is small relative to some tolerance  $\epsilon > 0$ . That is

$$\mathbb{E}_{\pi_Y} \left[ \mathcal{D}_{\text{KL}} \left( \pi_{X|Y}(\cdot|y) \parallel \pi_{X|Y}^*(\cdot|y) \right) \right] \leq \epsilon.$$

To find rotation matrices  $U$  and  $V$  and reduced dimensions  $r, s$  that minimize the posterior approximation error and satisfy the bound above, we use the following theorem from [4].

**Theorem 3.1 (Theorem 1 in [4]).** *Let  $X$  and  $Y$  be random variables whose joint distribution satisfies the logarithmic Sobolev inequality with constant  $C(\pi_{X,Y})$  as stated by Definition 2 in [4]. Then, we have*

$$\mathbb{E}_{\pi_Y} \left[ \mathcal{D}_{\text{KL}} \left( \pi_{X|Y}(\cdot|y) \parallel \pi_{X|Y}^*(\cdot|y) \right) \right] \leq C(\pi_{X,Y})^2 \left( \text{Tr}(U_{\perp}^{\top} H_X U_{\perp}) + \text{Tr}(V_{\perp}^{\top} H_Y V_{\perp}) \right),$$

for any unitary matrices  $U$  and  $V$ , where

$$(3.1) \quad H_X = \int \left( \nabla_x \nabla_y \log \pi_{Y|X}(y|x) \right)^{\top} \left( \nabla_x \nabla_y \log \pi_{Y|X}(y|x) \right) \pi_{X,Y}(x, y) dx dy$$

$$(3.2) \quad H_Y = \int \left( \nabla_x \nabla_y \log \pi_{Y|X}(y|x) \right) \left( \nabla_x \nabla_y \log \pi_{Y|X}(y|x) \right)^{\top} \pi_{X,Y}(x, y) dx dy.$$

Our goal is then to solve the following optimization problem:

$$\arg \min_{U_{\perp}^{\top}, V_{\perp}^{\top}} \text{Tr}(U_{\perp}^{\top} H_X U_{\perp}) + \text{Tr}(V_{\perp}^{\top} H_Y V_{\perp}),$$

subject to the constraints  $U_{\perp}^{\top} U_{\perp} = I_{n_x-r}$  and  $V_{\perp}^{\top} V_{\perp} = I_{n_y-s}$ . Following classical results in linear algebra,  $U_{\perp}$  are the eigenvectors corresponding to the smallest  $r$  eigenvalues of the matrix  $H_X$ . Similarly,  $V_{\perp}$  are the eigenvectors corresponding to the smallest  $s$  eigenvalues of the matrix  $H_Y$ .

**3.1. Gaussian prior and likelihood case.** If we have a Gaussian prior and likelihood, the previous derivation can be further simplified. Consider the following problem:

$$Y = G(X) + \mathcal{E},$$

where  $X \sim \mathcal{N}(0, \Sigma_X)$ ,  $\mathcal{E} \sim \mathcal{N}(0, \Sigma_{\mathcal{E}})$ , and  $G$  is the forward model. Let  $\tilde{X} = \Sigma_X^{-1/2} X$  and  $\tilde{Y} = \Sigma_{\mathcal{E}}^{-1/2} Y$  be pre-conditioned parameter and data variables. The connection between  $\tilde{Y}$  and  $\tilde{X}$  is given by

$$\tilde{Y} = \Sigma_{\mathcal{E}}^{-1/2} G(\Sigma_X^{1/2} \tilde{X}) + \Sigma_{\mathcal{E}}^{-1/2} \mathcal{E},$$

Using that  $\nabla_y \nabla_x \pi_{\tilde{Y}|\tilde{X}}(y|x) = \Sigma_{\mathcal{E}}^{-1/2} \nabla G(X) \Sigma_X^{1/2}$ , the diagnostic matrices in (3.1) and (3.2) are given by

$$(3.3) \quad H_{\tilde{X}} = \Sigma_X^{1/2} \left( \int \nabla G(X)^{\top} \Sigma_{\mathcal{E}}^{-1} \nabla G(X) \pi_X(x) dx \right) \Sigma_X^{1/2}$$

$$(3.4) \quad H_{\tilde{Y}} = \Sigma_{\mathcal{E}}^{-1/2} \left( \int \nabla G(X) \Sigma_X \nabla G(X)^{\top} \pi_X(x) dx \right) \Sigma_{\mathcal{E}}^{-1/2}.$$

Let  $\tilde{U}$  and  $\tilde{V}$  denote the matrices whose columns are the eigenvectors of  $H_{\tilde{X}}$  and  $H_{\tilde{Y}}$ , respectively. Then, we obtain the matrices  $U$  and  $V$  using

$$U = \Sigma_X^{-1/2} \tilde{U}, \quad V = \Sigma_{\mathcal{E}}^{-1/2} \tilde{V},$$

where  $\tilde{U}$  and  $\tilde{V}$  satisfy the properties  $\tilde{U}^\top \Sigma_X \tilde{U} = I$  and  $\tilde{V}^\top \Sigma_{\mathcal{E}} \tilde{V} = I$ . Let  $U_r$  and  $V_s$  be the matrices composed of the first  $r$  and  $s$  columns of  $U$  and  $V$ , respectively. The optimal projection, in terms of preserving mutual information, is given by  $X_r = U_r^\top X$  and  $Y_s = V_s^\top Y$ . We can then compute the mutual information  $\mathcal{I}(X_r, Y_s)$  in the reduced coordinates, and the error is proportional to  $\sum_{i=r+1}^{n_x} \lambda_i \left( U_\perp^\top H_X U_\perp \right) + \sum_{i=s+1}^{n_y} \lambda_i \left( V_\perp^\top H_Y V_\perp \right)$ , where  $\lambda_i$  denotes the  $i$ th largest eigenvalue of the corresponding matrix. For further details, see [4].

**3.2. Lower bounds of MI and the choice of estimators.** To reduce the dimensionality of the samples, we need access to the gradient of the forward model, specifically  $\nabla G(X)$ , which is not available in a completely likelihood-free setting. This limits us to using  $\widehat{\text{EIG}}_{\text{m}}$  and  $\widehat{\text{EIG}}_{\text{pos}}$ . In the rotated space, we define:

$$\begin{aligned} \widehat{\text{EIG}}_{\text{m}}(r, s) &= \frac{1}{M} \sum_{i=1}^M \log \frac{\pi_{Y_s|X_r}(y_s^i|x_r^i)}{\widehat{\pi}_{Y_s}(y_s^i)}, \\ \widehat{\text{EIG}}_{\text{pos}}(r, s) &= \frac{1}{M} \sum_{i=1}^M \log \frac{\widehat{\pi}_{X_r|Y_s}(x_r^i|y_s^i)}{\pi_{X_r}(x_r^i)}. \end{aligned}$$

Then note that  $\mathbb{E}_{\pi_{X_r, Y_s}} \left[ \log \frac{\widehat{\pi}_{X_r|Y_s}(x_r^i|y_s^i)}{\pi_{X_r}(x_r^i)} \right] \leq \mathcal{I}(X_r; Y_s) \leq \mathcal{I}(X; Y)$ , where the first inequality follows from the lower bound of the EIG, and the second is obtained from the data processing inequality. Therefore,  $\widehat{\text{EIG}}_{\text{pos}}$  serves as a lower bound in the asymptotic sense. However, the relationship between  $\widehat{\text{EIG}}_{\text{m}}(r, s)$  and the true EIG remains unclear. Although  $\mathbb{E}_{\pi_{X_r, Y_s}} \left[ \log \frac{\pi_{Y_s|X_r}(y_s^i|x_r^i)}{\widehat{\pi}_{Y_s}(y_s^i)} \right] \geq \mathcal{I}(X_r, Y_s)$ , it does not provide a clear upper or lower bound for  $\mathcal{I}(X, Y)$ . We thus focus on computing  $\widehat{\text{EIG}}_{\text{pos}}$  in high-dimensional settings. We summarize the proposed method for EIG estimation using low-dimensional projections in Algorithm 3.1.

---

**Algorithm 3.1** EIG estimation using low-dimensional projections

---

- 1: **Input:** Partition the  $L$  pairs of samples into  $N$  training and  $M$  evaluation samples, such that  $L = N + M$ ;  $\nabla G(X)$ ;  $\Sigma_X$ ;  $\Sigma_Y$ ;  $\Sigma_{\mathcal{E}}$ ; joint samples  $\{x^i, y^i\}_{i=1}^L$
  - 2: **Output:** EIG estimator
  - 3: Compute the diagnostic matrices  $H_{\tilde{X}}$  in (3.3) and  $H_{\tilde{Y}}$  in (3.4)
  - 4: Compute the leading  $r$  and  $s$  eigenvectors  $U_r$  and  $V_s$  of  $H_{\tilde{X}}$  and  $H_{\tilde{Y}}$ , respectively.
  - 5: Project parameter and data samples:  $x_r^i = U_r^\top x^i$ ,  $y_s^i = V_s^\top y^i$ .
  - 6: Use  $N$  training samples to learn the transport maps and obtain  $\widehat{\pi}_{X_r|Y_s}(x_r|y_s)$ .
  - 7: Use  $M$  pairs of samples to estimate EIG by evaluating the empirical average  $\widehat{\text{EIG}}_{\text{pos}} = \frac{1}{M} \sum_{i=1}^M \log \frac{\widehat{\pi}_{X_r|Y_s}(x_r^i|y_s^i)}{\pi_{X_r}(x_r^i)}$ .
- 

**4. Numerical Experiments.** In this section, we present three numerical examples to illustrate our proposed method. The first one is a linear Gaussian example, where we observe that the empirical convergence rate aligns with the theoretical convergence rate in the asymptotic regime. We then use a nonlinear example to demonstrate that our method performs well even when the joint distribution is non-Gaussian and the forward model is nonlinear. Finally, we consider a challenging nonlinear example with both data and parameters in high dimensions. We use our proposed dimension reduction technique to showcase our method's capability to handle EIG estimation

effectively in high-dimensional settings. Throughout this section, we use the following notations to indicate the empirical approximations of the corresponding EIG estimators:

$$\begin{aligned}\widehat{\text{EIG}}_{\text{m}} &= \frac{1}{M} \sum_{i=1}^M \log \frac{\pi_{Y|X}(y^i|x^i)}{\widehat{\pi}_Y(y^i)}, \\ \widehat{\text{EIG}}_{\text{pos}} &= \frac{1}{M} \sum_{i=1}^M \log \frac{\widehat{\pi}_{X|Y}(x^i|y^i)}{\pi_X(x^i)}, \\ \widehat{\text{EIG}}_{\text{lik}} &= \frac{1}{M} \sum_{i=1}^M \log \frac{\widehat{\pi}_{Y|X}(y^i|x^i)}{\widehat{\pi}_Y(y^i)}, \\ \widehat{\text{EIG}}_{\text{pr}} &= \frac{1}{M} \sum_{i=1}^M \log \frac{\widehat{\pi}_{X|Y}(x^i|y^i)}{\widehat{\pi}_X(x^i)}.\end{aligned}$$

**4.1. Sample allocations and convergence rates.** In this example, we consider a simple linear Gaussian problem where the EIG can be computed in closed form. We restrict our transport map to be affine functions of their inputs, which is sufficient to ensure Assumption 2.1 is satisfied for the Gaussian target distributions. We first compare the different estimators, including the nested Monte Carlo (NMC) estimator, against the analytical result. The forward model  $G: X \rightarrow Y$  is a random finite-dimensional linear map from  $\mathbb{R}^{20}$  to  $\mathbb{R}^{10}$  with prescribed eigenvalues  $\lambda_i = 0.8\lambda_{i-1}$ , where  $\lambda_1 = 1$ . The prior for  $X$  and additive noise  $\mathcal{E}$  are both multivariate Gaussian, i.e.,  $X \sim \mathcal{N}(0, \Sigma_X)$  and  $\mathcal{E} \sim \mathcal{N}(0, \Sigma_{\mathcal{E}})$ . We generate  $\Sigma_X$  using a squared exponential kernel given by  $\sigma \exp(-\|z_i - z_j\|^2/l^2)$ , where we set  $\sigma = 0.1$  and  $l = 0.1$ , and  $z_i$ 's are 20 equally spaced points between 0 and 1. We set  $\Sigma_{\mathcal{E}} = 0.01I_{10}$ . The true EIG is easily computed to be  $\frac{1}{2} \log \frac{\det(G\Sigma_X G^T + \Sigma_{\mathcal{E}})}{\det(\Sigma_{\mathcal{E}})}$  [62].

To investigate the effect of sample allocation, we set the ratio between the evaluation samples and training samples to be  $L^p$ , with  $p = \frac{1}{8}, \frac{1}{3}, \frac{3}{4}$  respectively, and each experiment is repeated 100 times. In the first study, we assume the model is known and the likelihood function can be evaluated exactly, and we estimate only the marginal distribution of  $Y$ . That is, we use  $\widehat{\text{EIG}}_{\text{m}}$ . We also compare the performance of transport map-based estimators with that of the NMC estimator, where the NMC estimator is computed using the optimal sample allocation discussed in [24]. We then plot the estimated EIG along with their bias, variance, and mean squared error (MSE) for the different estimators in Figure 1 and 2. We observe that when we set the ratio of  $M$  and  $N$  to be proportional to  $L^{1/3}$ , the MSE decreases most rapidly as the total number of samples increases. The empirical convergence rate also aligns with the theory presented in the previous section. Next, we show in Figures 3 and 4 that by fixing the prior and using transport maps to approximate the posterior density, i.e., setting the EIG estimator to  $\widehat{\text{EIG}}_{\text{pos}}$ , we achieve the same rate.

We then study the likelihood-free case, where we estimate either the likelihood and the marginal densities and obtain  $\widehat{\text{EIG}}_{\text{lik}}$  (Figure 5), or the posterior and prior densities and obtain  $\widehat{\text{EIG}}_{\text{pr}}$  (Figure 7). As shown in Figures 6 and 8, in both cases, the convergence rate of the MSE of the transport map-based EIG estimator matches the theoretical rate ( $O(L^{-1})$ ) in the asymptotic regime, which is faster than that of the NMC ( $O(L^{-2/3})$ ).

We then present a few observations: The convergence rate of the MSE with sample allocation  $\frac{M}{N} \sim O(L^{1/3})$  is of order  $L^{-1}$  in the asymptotic region across all four cases. For  $L^p$ , when  $p > \frac{1}{2}$ , we observe that the convergence rate of the MSE is considerably slower than for  $p \leq \frac{1}{2}$  in all four cases, which supports our theoretical results developed in Subsection 2.3. From the violin plot, we see that all the transport map-based results have smaller variance than NMC, and with allocation

ratios of  $L^{1/8}$  and  $L^{1/3}$ , transport maps produce good results even with small sample sizes. Another noteworthy observation is that  $\widehat{\text{EIG}}_{\text{lik}}$  and  $\widehat{\text{EIG}}_{\text{pr}}$  exhibit the same values, up to numerical error (see Figures 5 and 7). This occurs because we are in the linear Gaussian case, and if we assume the mean has been shifted to 0, then the map can be computed from covariance matrix of the joint samples. In other words, we can obtain  $\widehat{\pi}_Y$ ,  $\widehat{\pi}_{Y|X}$ ,  $\widehat{\pi}_X$ , and  $\widehat{\pi}_{X|Y}$  directly from the sample covariance matrix of the joint distribution. Therefore, we have exactly  $\frac{\widehat{\pi}_{X|Y}(x|y)}{\widehat{\pi}_X(x)} = \frac{\widehat{\pi}_{Y|X}(y|x)}{\widehat{\pi}_Y(y)}$  for any  $x$  and  $y$ .

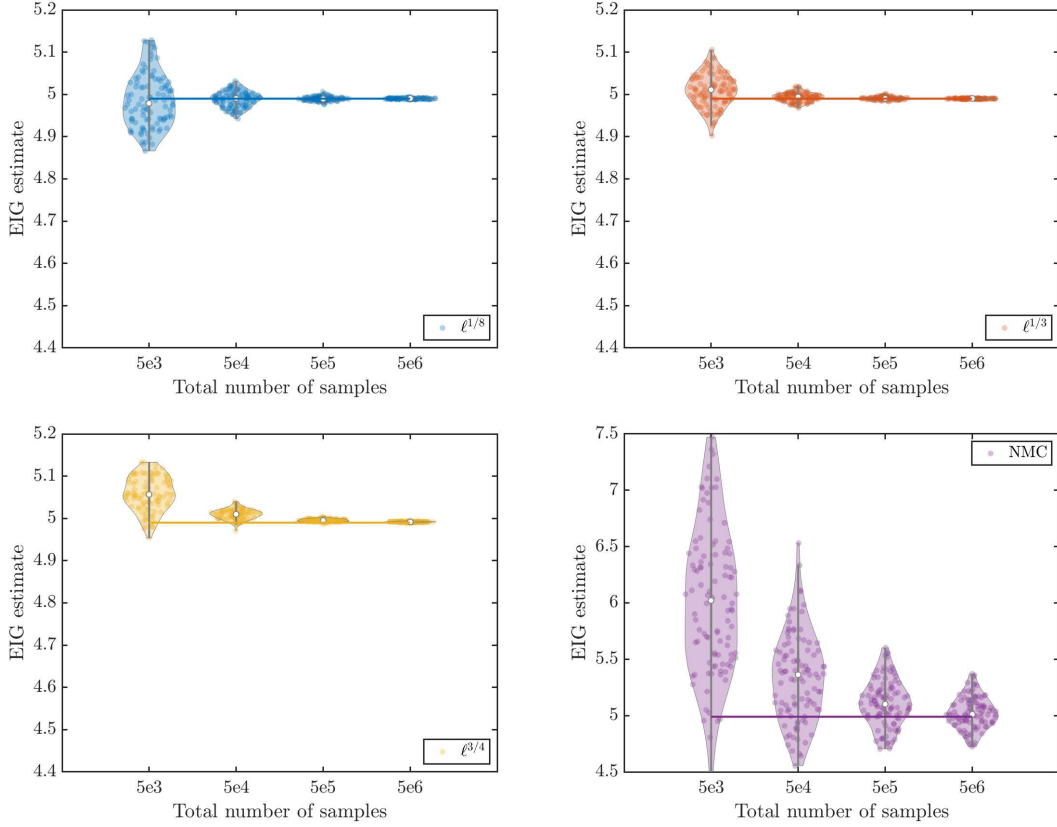


Figure 1: The violin plot of  $\widehat{\text{EIG}}_m$ , with different ratios between the number of training and evaluation samples. The solid line denotes the EIG value computed from the closed-form expression.

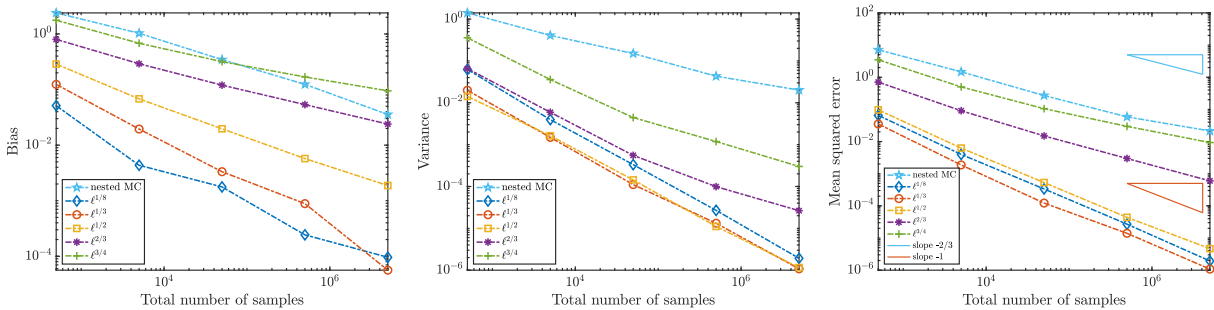


Figure 2: Convergence of the bias, variance, and MSE of  $\widehat{\text{EIG}}_m$ .

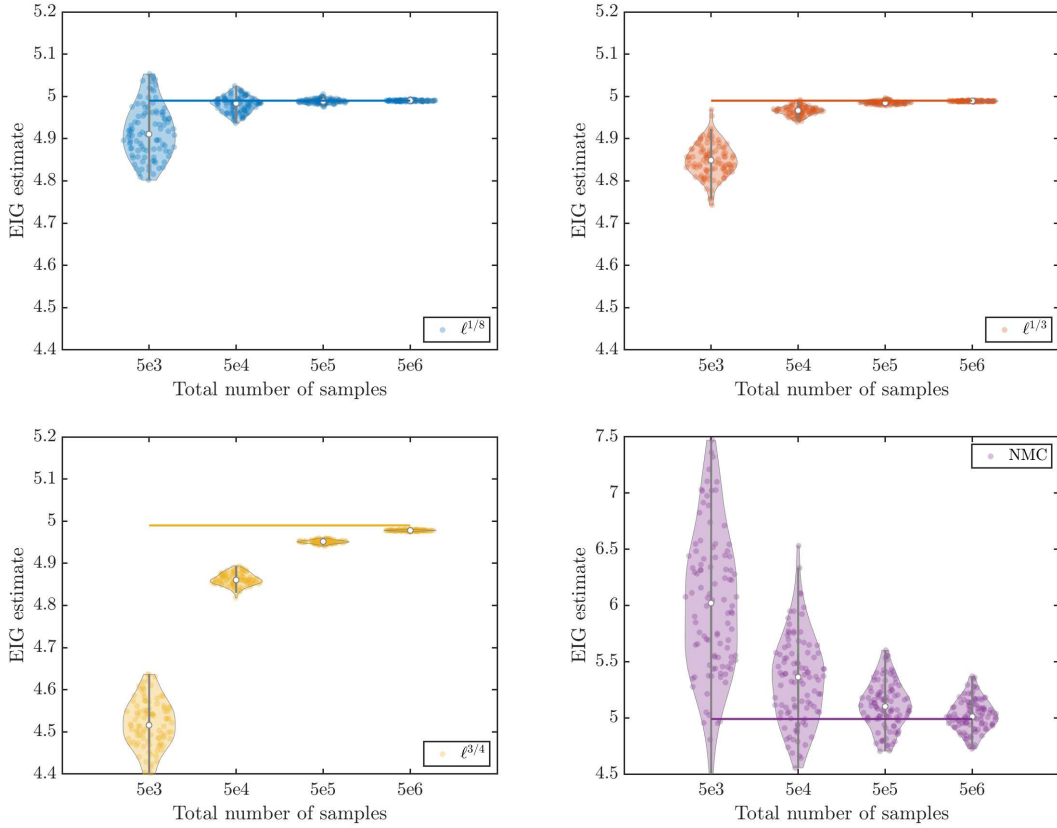


Figure 3: The violin plot of  $\widehat{\text{EIG}}_{\text{pos}}$ , with different ratios between the number of training and evaluation samples. The solid line denotes the EIG value computed from the closed-form expression.

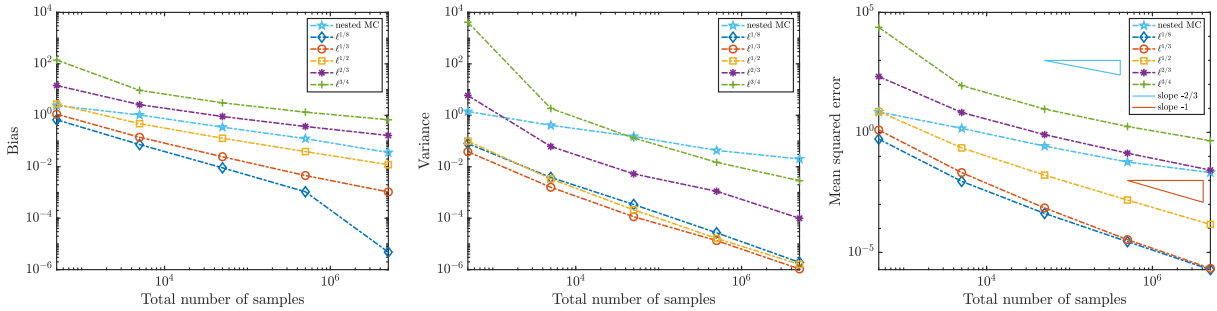


Figure 4: Convergence of the bias, variance, and MSE of  $\widehat{\text{EIG}}_{\text{pos}}$ .

**4.2. Transport-based estimators of focused and full EIG.** We then study a nonlinear example, Mössbauer spectroscopy, to demonstrate the flexibility of transport maps. Mössbauer spectroscopy is a technique that leverages the Mössbauer effect, which refers to the nearly recoil-free emission and absorption of gamma radiation in solids. This technique is used to discover isomer shifts, quadrupole splitting, and magnetic Zeeman splitting. A detailed description of the model can be found in [24] and [44]. The parameters in this model are “center”, “width”, “height”, and “offset”. The absorption peak is modeled using a Lorentzian profile, as per the standard parameterization

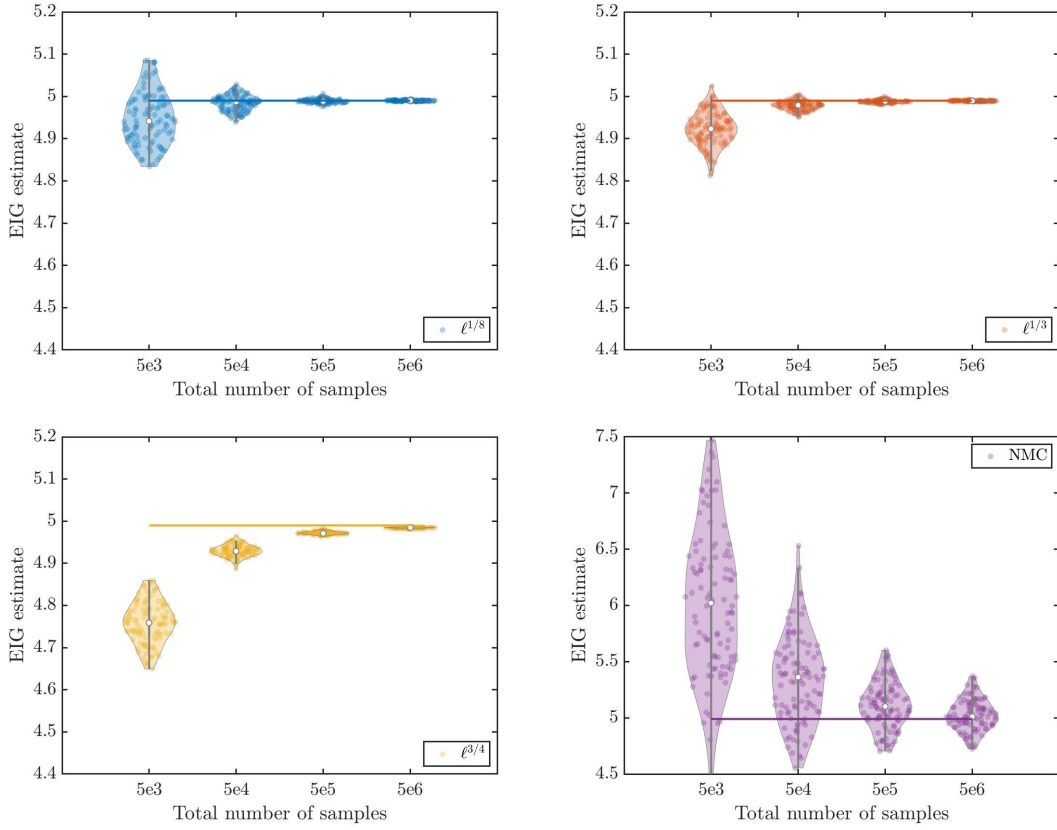


Figure 5: The violin plot of  $\widehat{\text{EIG}}_{\text{lik}}$ , with different ratios between the number of training and evaluation samples. The solid line denotes the EIG value computed from the closed-form expression.

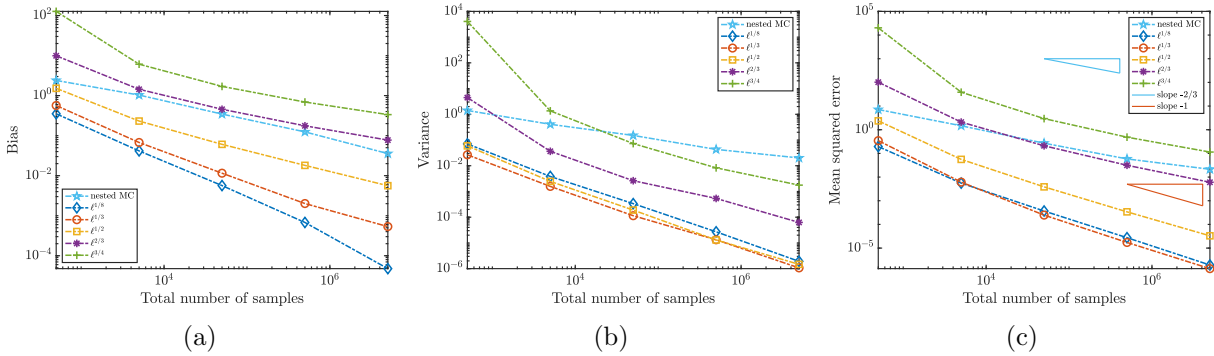


Figure 6: Convergence of the bias, variance, and MSE of  $\widehat{\text{EIG}}_{\text{lik}}$ .

described in [29]. This allows the number of detector counts  $y_i$  at a given velocity  $d$  to be expressed by the following equation,

$$Y_i(d; \cdot) = \text{offset} - \text{height} \frac{\text{width}^2}{\text{width}^2 + (\text{center} - d)^2} + \mathcal{E}_i,$$

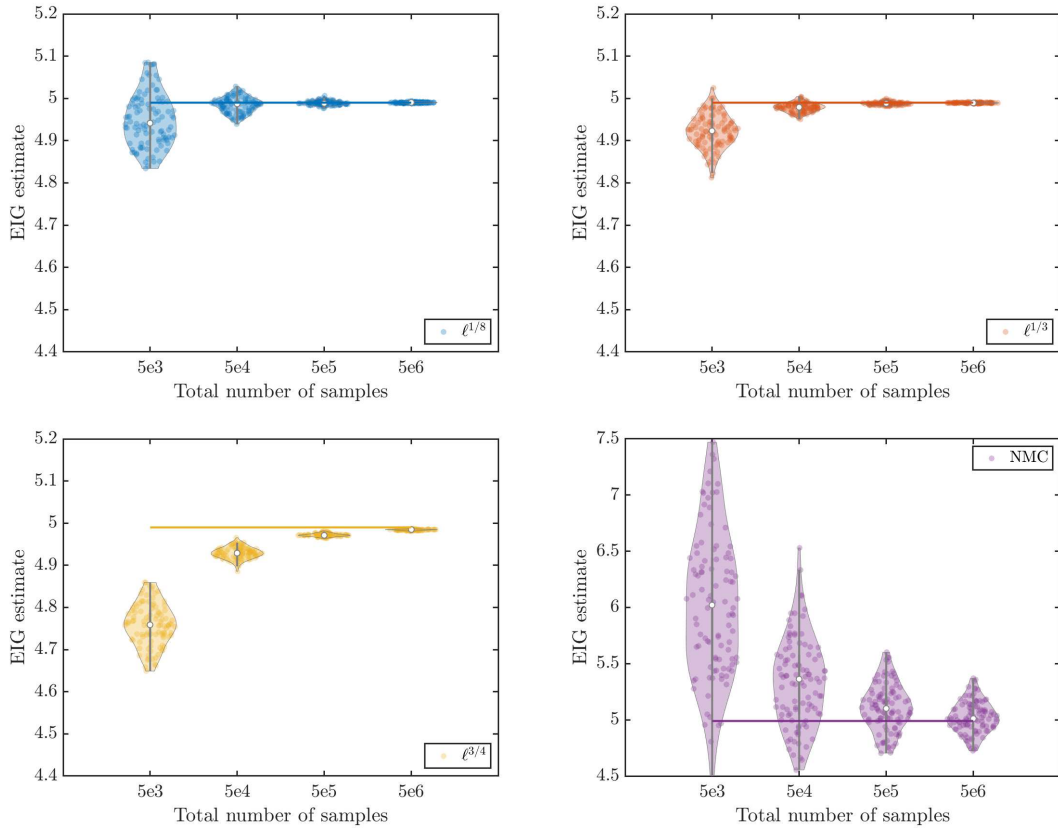


Figure 7: The violin plot of  $\widehat{\text{EIG}}_{\text{pr}}$ , with different ratios between the number of training and evaluation samples. The solid line denotes the EIG value computed from the closed-form expression.

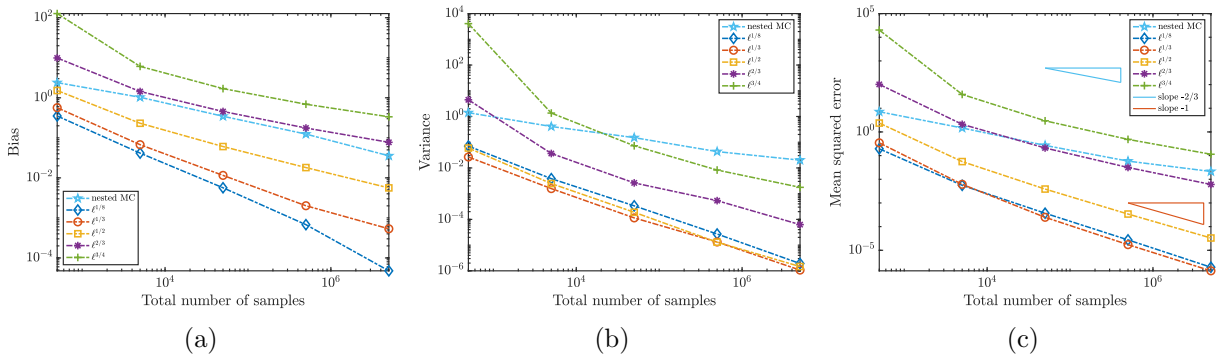


Figure 8: Convergence of the bias, variance, and MSE of  $\widehat{\text{EIG}}_{\text{pr}}$ .

and the parameters of the model are distributed according to the following priors:

$$\begin{aligned} \text{center} &\sim \mathcal{N}(0, 1), \\ \log(\text{width}) &\sim \mathcal{N}(0, 0.3^2), \\ \log(\text{height}) &\sim \mathcal{N}(0, 0.3^2), \\ \log(\text{offset}) &\sim \mathcal{N}(1.0, 0.2^2). \end{aligned}$$

The additive noise is assumed to be Gaussian, with  $\mathcal{E}_i \sim \mathcal{N}(0, 0.1^2)$ , and  $d = [-1.3, 0, 1.3]$ . For convenience, we rename the center, width, height, and offset as  $X_1$ ,  $X_2$ ,  $X_3$ , and  $X_4$ , respectively. First, we note that this model is highly nonlinear, as evidenced by the joint distribution of the samples. While all the  $X_i$ 's (or their logarithms) are jointly Gaussian, the joint distribution of the  $Y_i$ 's and the joint distribution between the  $Y_i$ 's and  $X_i$ 's deviate significantly from being Gaussian (see Figure 9).

We then consider the problem of estimating the following two quantities:  $\mathcal{I}(X_1; Y)$  and  $\mathcal{I}(X; Y)$ , which we refer to as the ‘‘focused’’ and ‘‘full’’ cases, respectively. In each case, we apply both non-likelihood-free and likelihood-free methods. For the focused case, we study the following three EIG estimators:

$$\begin{aligned} \widehat{\text{EIG}}_{\text{pos}} &= \frac{1}{M} \sum_{i=1}^M \log \frac{\widehat{\pi}_{X_1|Y}(x_1^i|y^i)}{\pi_{X_1}(x_1^i)}, \\ \widehat{\text{EIG}}_{\text{pr}} &= \frac{1}{M} \sum_{i=1}^M \log \frac{\widehat{\pi}_{X_1|Y}(x_1^i|y^i)}{\widehat{\pi}_{X_1}(x_1^i)}, \\ \widehat{\text{EIG}}_{\text{lik}} &= \frac{1}{M} \sum_{i=1}^M \log \frac{\widehat{\pi}_{Y|X_1}(y^i|x_1^i)}{\widehat{\pi}_Y(y^i)}. \end{aligned}$$

All densities are estimated using  $N$  pairs of samples. We set the ‘‘ground truth’’ to be the EIG estimator obtained using NMC. To obtain a consistent estimator of EIG using Monte Carlo for the focused case, we employed layered multiple importance sampling (LMIS) from [24] with  $1.58 \times 10^6$  samples (5623 for the outer loops and 281 for the inner loops). For the full case, we used the NMC algorithm with  $10^{10}$  samples, where the allocation of samples between the inner and outer loops is determined using the optimal allocation proposed in [24]. In this case, we have  $3.83 \times 10^6$  samples for the inner loop and 2610 for the outer loop. We repeated the procedure 10 times to calculate the mean and variance of the EIG estimators obtained using LMIS and NMC. The mean of the Monte Carlo estimators in the focused and full cases is 1.54 and 4.52 respectively, with corresponding variances of  $4.73 \times 10^{-5}$  and  $4.59 \times 10^{-4}$ . We then obtained EIG estimators using transport maps with an increasing total number of samples: 500, 5000, and 50000, and with the number of training and evaluation samples split according to the optimal sample allocation  $M/N \sim O(L^{1/3})$ , as derived in the previous section. We repeated the experiments, and obtained 30 transport map-based EIG estimators. We present the numerical results of both cases in Figures 10 and 11.

From the plots, we observe that as the number of samples increases, the EIG estimates converge to the ground truth and the variance decreases considerably in both cases. The performance in the focused case is generally better since we only need to estimate a 4-dimensional map, whereas in the full case, we need to estimate a 7-dimensional map. If we estimate EIG using Monte Carlo, the focused case is more challenging, as it requires a specially designed algorithm (LMIS). Note that in 11c, we can see that both estimators converge to the truth. Since nested MC is positively biased, the true EIG is likely between 4.1 and 4.5.

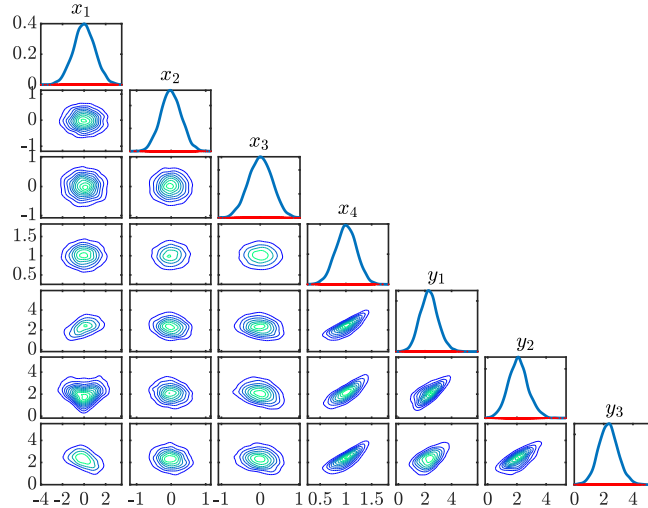


Figure 9: Original samples from the joint distribution before applying transport maps

Finally, we present the joint distribution after applying the transport maps in Figure 12a. As seen, the joint distribution after the push-forward map is very close to a standard normal distribution. To further illustrate the Gaussianity of the push-forward samples, we present the quantile-quantile plot (Q–Q plot) of the push-forward samples against that of a standard normal. To be precise, we generate 20 random vectors of unit length, and project 7-dimensional data onto 20 random directions, respectively. We then plot the quantile of these random projections against that of a standard normal distribution. If the push-forward distribution is exactly Gaussian, the Q–Q plot of the random projections would align with the black line (see Box 2.4 in [57]). As shown in Figure 12b, only the tails of the push-forward samples deviate slightly, demonstrating the effectiveness of transport maps in transforming highly non-Gaussian samples into a standard Gaussian distribution.

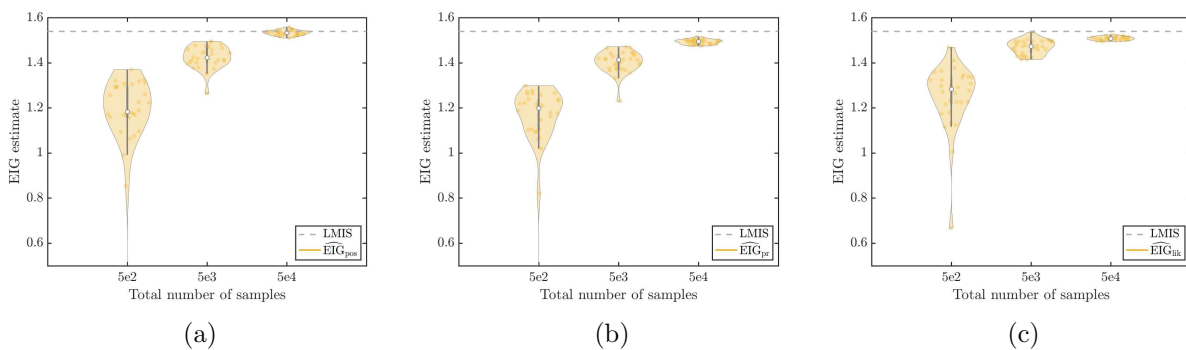


Figure 10: Convergence of different EIG estimators in the focused case: (a)  $\widehat{\text{EIG}}_{\text{pos}}$ ; (b)  $\widehat{\text{EIG}}_{\text{pr}}$ ; (c)  $\widehat{\text{EIG}}_{\text{lik}}$ . The dashed line represents the “ground truth” obtained using LMIS.

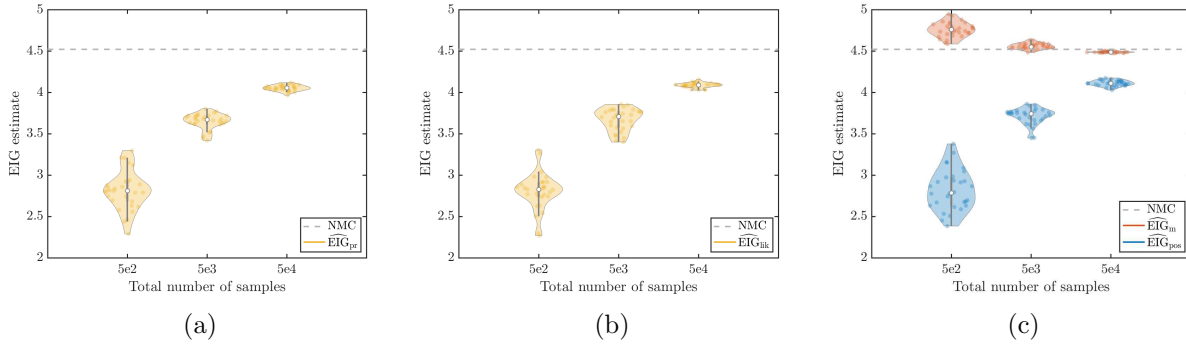


Figure 11: Convergence of different EIG estimators in the full case: (a)  $\widehat{\text{EIG}}_{\text{pr}}$ ; (b)  $\widehat{\text{EIG}}_{\text{lik}}$ ; (c)  $\widehat{\text{EIG}}_{\text{m}}$  and  $\widehat{\text{EIG}}_{\text{pos}}$ . The dashed line represents the “ground truth” obtained using NMC.

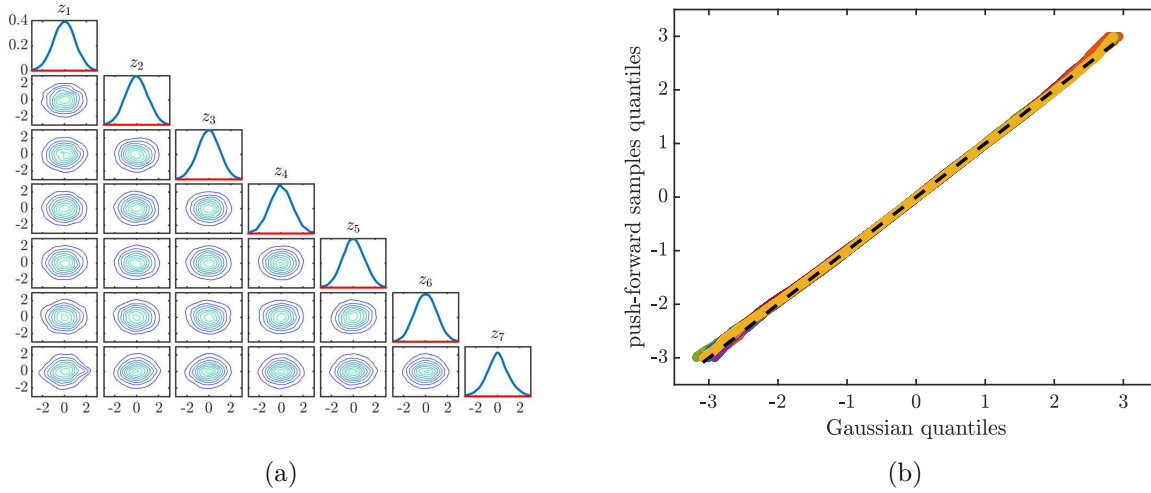


Figure 12: (a) Push-forward joint densities after applying transport maps; (b) Push-forward samples shown using Q-Q plot

**4.3. EIG estimation in high dimensions: linear elasticity inverse problem.** In this problem, we compare the proposed dimension reduction method for EIG estimation, referred to as Conditional Mutual Information (CMI), to alternative methods based on Principal Component Analysis (PCA) [30] and Canonical Correlation Analysis (CCA) [31]. We consider the problem of estimating mutual information between the Young’s modulus field in a wrench-shaped domain and a noisy observation of its displacement on the upper boundary after applying an external force to a subset of the boundary  $\partial\Omega$ . Following the setup in [4, 39, 58], the displacement  $u : \Omega \rightarrow \mathbb{R}^2$  is related to the Young’s modulus  $E : \Omega \rightarrow \mathbb{R}_{\geq 0}$  through the partial differential equation

$$\nabla \cdot (K : \epsilon(u)) = 0,$$

where

$$K : \epsilon(u) = \frac{E}{1 + \nu} \epsilon(u) + \frac{\nu E}{1 - \nu^2} \text{Tr}(\epsilon(u)) I_2,$$

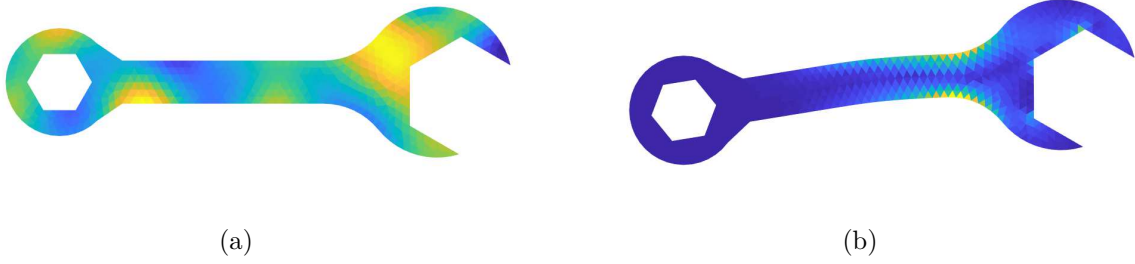


Figure 13: A realization of the parameter and solution field

and  $\nu = 0.3$  is the Poisson's ratio. The wrench is clamped at its right end, experiencing no displacement, i.e.,  $u = 0$ . The Young's modulus field is assumed to have a log-normal prior distribution, specifically  $\log E \sim \mathcal{N}(0, C)$ , where  $C$  is a squared exponential covariance kernel given by  $C(z_1, z_2) = \exp(-\|z_1 - z_2\|^2)$  with  $z_1, z_2 \in \Omega$ . The domain is discretized with 925 elements using the finite element method, resulting  $X \in \mathbb{R}^{925}$ . The observation operator  $D$  maps the Galerkin solution  $u^h$  to a subset of 26 dimensions. We then write  $Y = G(X) + \mathcal{E}$ , where  $G = Du^h(X)$ , and  $\mathcal{E} \sim \mathcal{N}(0, DR^{-1}D^\top)$ , with  $R$  being the Riesz map associated with the  $H^1(\Omega)$  norm, such that  $\|u^h\|_R^2 = \int_\Omega (u^h(s))^2 + \|\nabla u^h(s)\|^2 ds$  [72]. Figure 13 displays a realization of the parameter and the solution field.

To compare the EIG estimators using different dimension reduction schemes, we use 500 samples to estimate  $H_X$  and  $H_Y$ , and then compute the eigenvectors associated with these two matrices. Additionally, we compute the eigenvectors obtained through PCA and CCA. Recall that the principal component associated with PCA solves the following eigenvalue problem,

$$\begin{aligned}\Sigma_X u^{\text{PCA}} &= \lambda_X u^{\text{PCA}} \\ \Sigma_Y v^{\text{PCA}} &= \lambda_Y v^{\text{PCA}}.\end{aligned}$$

One the other hand, CCA finds the maximal correlation over all possible linear transformations of two multivariate random variables. The corresponding eigenvalue problem writes:

$$\begin{aligned}\Sigma_{XY} \Sigma_Y^{-1} \Sigma_{YX} u^{\text{CCA}} &= \rho \Sigma_X u^{\text{CCA}} \\ \Sigma_{YX} \Sigma_X^{-1} \Sigma_{XY} v^{\text{CCA}} &= \rho \Sigma_Y v^{\text{CCA}}.\end{aligned}$$

We then transform the samples  $x^i$  and  $y^i$  using these eigenvectors  $\{u^{\text{CMI}}, v^{\text{CMI}}\}, \{u^{\text{PCA}}, v^{\text{PCA}}\}$ , and  $\{u^{\text{CCA}}, v^{\text{CCA}}\}$ , respectively, where  $\{u^{\text{CMI}}, v^{\text{CMI}}\}$  is computed following Algorithm 3.1. The maps are trained using  $N = 2500$  samples. We then compute the Monte Carlo average using  $M = 10000$  evaluation samples to obtain the estimator  $\frac{1}{M} \sum_{i=1}^M \frac{\hat{\pi}_{X_r|Y_s}(x_r^i|y_s^i)}{\pi_{X_r}(x_r^i)}$ . To illustrate the effectiveness of our proposed nonlinear dimension reduction method, we compute the EIG as if the data were Gaussian. To be precise, we compute the EIG using the formula  $\frac{1}{2} \log \frac{\det(\hat{\Sigma}_X) \det(\hat{\Sigma}_Y)}{\det(\hat{\Sigma}_{X,Y})}$ . Here,  $\hat{\Sigma}_X, \hat{\Sigma}_Y$  and  $\hat{\Sigma}_{X,Y}$  denote the sample covariance of  $X, Y$  and the joint distribution of  $X$  and  $Y$ , respectively. In practice, covariance matrices are approximated using their empirical counterparts estimated using 10000 samples. For reproducibility, the same experiment is repeated 10 times, and we show the error bars, representing two standard error of the mean in Figure 14.

The ground truth in this case is unknown. However, we know that the EIG estimator used in this case serves as a lower bound to the true EIG. Therefore, the best EIG estimators should

dominate others. We present the mean of EIG estimators and its associated error in Appendix D. In Figure 14, we plot the convergence results with  $r = s = 1$  to  $r = s = 8$ . As we can see, using CMI for dimension reduction yields the highest value, hence giving the best performance. The results obtained using the Gaussian approximation, on the other hand, perform worse than their corresponding counterparts obtained using transport maps, illustrating the flexibility of transport maps in handling non-Gaussian data. To demonstrate the comparison in detail, we further compute the EIG using the Gaussian approximation by holding the dimension of  $X_r$  constant at  $r = 300$  and varying the dimension of  $Y_s$  from  $s = 1$  to  $s = 26$ . Then, we hold the dimension of  $Y_s$  constant at  $s = 26$  and vary the dimension of  $X_r$  from  $r = 1$  to  $r = 300$ . The results are presented in Figure 15, with the shaded region indicating two standard errors of the mean. As we can see, for PCA and CMI, the performance is inferior when using the Gaussian approximation, even when the retained dimension is high. This further suggests the necessity of combining nonlinear dimension reduction techniques with non-Gaussian methods for EIG estimation: one can achieve better performance with a more flexible framework and significantly more truncated dimensions, than a crude method with less truncation. It is also interesting to note that the benefit is greatest when the bases obtained from CMI for dimension reduction. This suggests that the nonlinearity of the parameters and the data is largely captured by selecting the appropriate bases for estimating mutual information. Further exploration of this phenomenon will be included in future work.

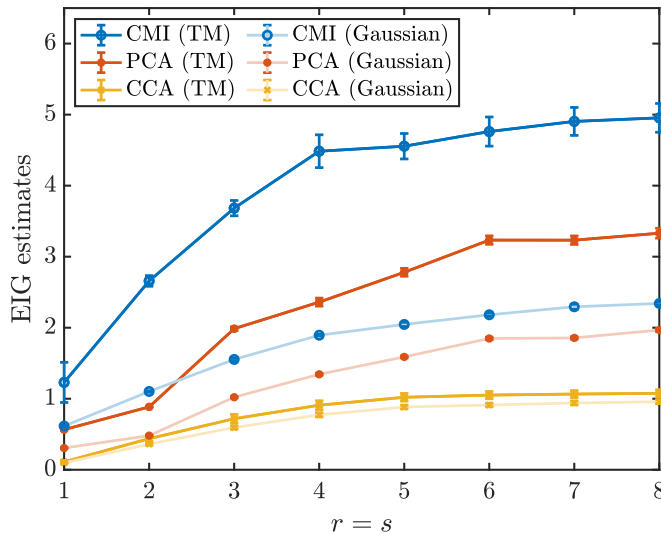


Figure 14: EIG estimates using transport maps and Gaussian, with truncated dimensions using CMI, PCA, and CCA for  $r = s = 1$  to 8

**5. Conclusion.** In this paper, we study a key problem in Bayesian optimal experimental design — EIG estimation. We introduced the transport-map based method for EIG estimation in Section 2. This enables us to estimate EIG with both explicit and implicit models. In Subsection 2.3, we study the optimal sample allocation between the training and the evaluation samples for the purpose of minimizing the MSE. This is further verified with the linear Gaussian example presented in Subsection 4.1. In Section 3, we adopt the optimal dimension reduction technique from [4], enabling EIG to be estimated in high-dimensional settings. The numerical example presented in Section 4 show that our proposed method performs similarly comparing to nested Monte Carlo in terms of

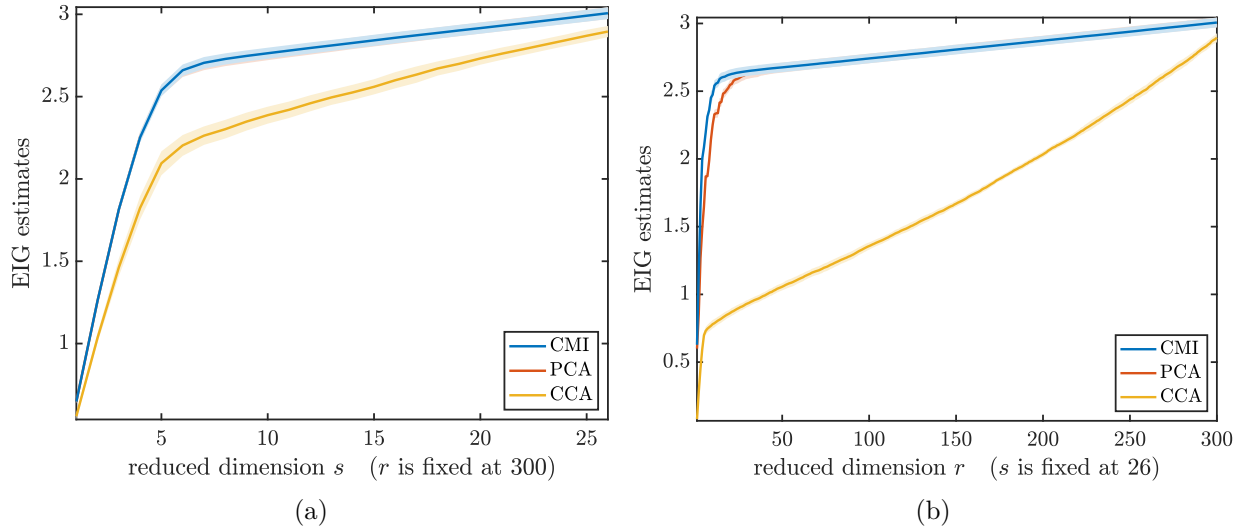


Figure 15: EIG estimates using Gaussian approximation, with truncated dimensions using CMI, PCA, and CCA

the EIG but with a much cheaper cost. We also demonstrate the performance of our method in the high-dimensional setting in [Subsection 4.3](#). The dimension reduction technique proposed in this paper outperform PCA, CCA, and its Gaussian counterpart in terms of EIG estimation.

For future work and directions, we would like to analyze the error in EIG estimation by considering a non-parametric approximation of the transport maps using the techniques presented in this paper [66]. In addition, we would also like to build transport maps that incorporates the design variable  $d$ , making this framework suitable for the Bayesian optimal experimental design problem.

**Acknowledgements.** RB is grateful for support from the von Kármán instructorship at Caltech, the Air Force Office of Scientific Research MURI on “Machine Learning and Physics-Based Modeling and Simulation” (award FA9550-20-1-0358) and a Department of Defense (DoD) Vannevar Bush Faculty Fellowship (award N00014-22-1-2790) held by Andrew M. Stuart.

## REFERENCES

- [1] Ahmed Attia, Alen Alexanderian, and Arvind K Saibaba. Goal-oriented optimal design of experiments for large-scale Bayesian linear inverse problems. *Inverse Problems*, 34(9):095009, 2018.
- [2] Ricardo Baptista, Lianghao Cao, Joshua Chen, Omar Ghattas, Fengyi Li, Youssef M. Marzouk, and J. Tinsley Oden. Bayesian model calibration for block copolymer self-assembly: Likelihood-free inference and expected information gain computation via measure transport. *Journal of Computational Physics*, 503:112844, 2024.
- [3] Ricardo Baptista, Bamdad Hosseini, Nikola B Kovachki, and Youssef M Marzouk. Conditional sampling with monotone gans: from generative models to likelihood-free inference. *SIAM/ASA Journal on Uncertainty Quantification*, 12(3):868–900, 2024.
- [4] Ricardo Baptista, Youssef Marzouk, and Olivier Zahm. Gradient-based data and parameter dimension reduction for Bayesian models: an information theoretic perspective. *arXiv:2207.08670*, 2022.
- [5] Ricardo Baptista, Youssef Marzouk, and Olivier Zahm. On the representation and learning of monotone triangular transport maps. *Foundations of Computational Mathematics*, pages 1–46, 2023.
- [6] Joakim Beck, Ben Mansour Dia, Luis Espath, and Raúl Tempone. Multilevel double loop Monte Carlo and stochastic collocation methods with importance sampling for Bayesian optimal experimental design. *International Journal for Numerical Methods in Engineering*, 121(15):3482–3503, 2020.
- [7] Mohamed Ishmael Belghazi, Aristide Baratin, Sai Rajeshwar, Sherjil Ozair, Yoshua Bengio, Aaron Courville, and Devon Hjelm. Mutual information neural estimation. In Jennifer Dy and Andreas Krause, editors,

- Proceedings of the 35th International Conference on Machine Learning*, volume 80 of *Proceedings of Machine Learning Research*, pages 531–540. PMLR, 10–15 Jul 2018.
- [8] Jose M. Bernardo. Expected Information as Expected Utility. *The Annals of Statistics*, 7(3):686 – 690, 1979.
  - [9] Steffen Bickel, Michael Brückner, and Tobias Scheffer. Discriminative learning for differing training and test distributions. In *Proceedings of the 24th international conference on Machine learning*, pages 81–88, 2007.
  - [10] Vladimir Igorevich Bogachev, Aleksandr Viktorovich Kolesnikov, and Kirill Vladimirovich Medvedev. Triangular transformations of measures. *Sbornik: Mathematics*, 196(3):309, 2005.
  - [11] Michael Brennan, Daniele Bigoni, Olivier Zahm, Alessio Spantini, and Youssef Marzouk. Greedy inference with structure-exploiting lazy maps. *Advances in Neural Information Processing Systems*, 33:8330–8342, 2020.
  - [12] G. Carlier, A. Galichon, and F. Santambrogio. From knothe’s transport to brenier’s map and a continuation method for optimal transport. *SIAM Journal on Mathematical Analysis*, 41(6):2554–2576, 2010.
  - [13] George Casella and Roger L Berger. *Statistical inference*, volume 2. Duxbury Pacific Grove, CA, 2002.
  - [14] Atlanta Chakraborty, Xun Huan, and Tommie Catanach. A likelihood-free approach to goal-oriented bayesian optimal experimental design, 2024.
  - [15] Kathryn Chaloner and Isabella Verdinelli. Bayesian Experimental Design: A Review. *Statistical Science*, 10(3):273 – 304, 1995.
  - [16] Kristy Choi, Madeline Liao, and Stefano Ermon. Featurized density ratio estimation, 2021.
  - [17] Kyle Cranmer, Johann Brehmer, and Gilles Louppe. The frontier of simulation-based inference. *Proceedings of the National Academy of Sciences*, 117(48):30055–30062, 2020.
  - [18] Tiangang Cui and Sergey Dolgov. Deep composition of tensor-trains using squared inverse rosenblatt transports. *Foundations of Computational Mathematics*, 22(6):1863–1922, 2022.
  - [19] Tiangang Cui, Karina Koval, Roland Herzog, and Robert Scheichl. Subspace accelerated measure transport methods for fast and scalable sequential experimental design, with application to photoacoustic imaging, 2025.
  - [20] Tiangang Cui, James Martin, Youssef M Marzouk, Antti Solonen, and Alessio Spantini. Likelihood-informed dimension reduction for nonlinear inverse problems. *Inverse Problems*, 30(11):114015, 2014.
  - [21] Tiangang Cui and Olivier Zahm. Data-free likelihood-informed dimension reduction of bayesian inverse problems. *Inverse Problems*, 37(4):045009, mar 2021.
  - [22] Holger Dette. A note on Bayesian c- and D-optimal designs in nonlinear regression models. *The Annals of Statistics*, 24(3):1225 – 1234, 1996.
  - [23] Jiayuan Dong, Christian Jacobsen, Mehdi Khalloufi, Maryam Akram, Wanjiao Liu, Karthik Duraisamy, and Xun Huan. Variational Bayesian optimal experimental design with normalizing flows. *arXiv preprint arXiv:2404.13056*, 2024.
  - [24] Chi Feng and Youssef M. Marzouk. A layered multiple importance sampling scheme for focused optimal Bayesian experimental design. *arXiv: 1903.11187*, 2019.
  - [25] G B Folland. Higher-Order Derivatives and Taylor’s Formula in Several Variables. <https://sites.math.washington.edu/~folland/Math425/taylor2.pdf>.
  - [26] Adam Foster, Martin Jankowiak, Elias Bingham, Paul Horsfall, Yee Whye Teh, Thomas Rainforth, and Noah Goodman. Variational Bayesian optimal experimental design. In *Advances in Neural Information Processing Systems*, volume 32, 2019.
  - [27] Weihao Gao, Sreeram Kannan, Sewoong Oh, and Pramod Viswanath. Estimating mutual information for discrete-continuous mixtures. In I. Guyon, U. Von Luxburg, S. Bengio, H. Wallach, R. Fergus, S. Vishwanathan, and R. Garnett, editors, *Advances in Neural Information Processing Systems*, volume 30. Curran Associates, Inc., 2017.
  - [28] Loïc Giraldi, Olivier P. Le Maître, Ibrahim Hoteit, and Omar M. Knio. Optimal projection of observations in a Bayesian setting. *Computational Statistics & Data Analysis*, 124:252–276, 2018.
  - [29] J. Hesse. Simple Arrangement for Educational Mössbauer-Effect Measurements. *American Journal of Physics*, 41(1):127–129, January 1973.
  - [30] Harold Hotelling. Analysis of a complex of statistical variables into principal components. *Journal of Educational Psychology*, 24:498–520, 1933.
  - [31] Harold Hotelling. Relations between two sets of variates. *Biometrika*, 28(3-4):321–377, 12 1936.
  - [32] Xun Huan, Jayanth Jagalur, and Youssef Marzouk. Optimal experimental design: Formulations and computations. *arXiv:2407.16212*, 2024.
  - [33] Jayanth Jagalur-Mohan and Youssef Marzouk. Bayesian optimal experimental design in non-submodular settings: batch algorithms and guarantees. *Preprint*, 2016.
  - [34] Noble Kennamer, Steven Walton, and Alexander Ihler. Design amortization for bayesian optimal experimental design, 2022.
  - [35] Steven Kleinegesse and Michael U. Gutmann. Efficient bayesian experimental design for implicit models. In *AISTATS*, 2019.

- [36] Karina Koval, Roland Herzog, and Robert Scheichl. Tractable optimal experimental design using transport maps. *ArXiv*, abs/2401.07971, 2024.
- [37] Alexander Kraskov, Harald Stögbauer, and Peter Grassberger. Estimating mutual information. *Phys. Rev. E*, 69:066138, Jun 2004.
- [38] Andreas Krause, Ajit Singh, and Carlos Guestrin. Near-optimal sensor placements in gaussian processes: Theory, efficient algorithms and empirical studies. *J. Mach. Learn. Res.*, 9:235–284, June 2008.
- [39] Remi R Lam, Olivier Zahm, Youssef M Marzouk, and Karen E Willcox. Multifidelity dimension reduction via active subspaces. *SIAM Journal on Scientific Computing*, 42(2):A929–A956, 2020.
- [40] Nunzio Alexandro Letizia, Nicola Novello, and Andrea M. Tonello. Variational f-divergence and derangements for discriminative mutual information estimation. *ArXiv*, abs/2305.20025, 2023.
- [41] D. V. Lindley. On a Measure of the Information Provided by an Experiment. *The Annals of Mathematical Statistics*, 27(4):986 – 1005, 1956.
- [42] Youssef Marzouk, Tarek Moselhy, Matthew Parno, and Alessio Spantini. *Sampling via Measure Transport: An Introduction*, pages 785–825. Springer International Publishing, Cham, 2016.
- [43] Daniel J. McDonald. Minimax density estimation for growing dimension. In *International Conference on Artificial Intelligence and Statistics*, 2017.
- [44] Rudolf L Mössbauer. Kernresonanzfluoreszenz von gammastrahlung in ir 191. *Zeitschrift für Physik*, 151(2):124–143, 1958.
- [45] XuanLong Nguyen, Martin Wainwright, and Michael Jordan. Estimating divergence functionals and the likelihood ratio by convex risk minimization. *Information Theory, IEEE Transactions on*, 56:5847 – 5861, 12 2010.
- [46] Kayode Ogungbenro, Aristides Dokoumetzidis, and Leon Aarons. Application of optimal design methodologies in clinical pharmacology experiments. *Pharmaceutical Statistics*, 8(3):239–252, 2009.
- [47] Rafael Orozco, Ali Siahkoobi, Gabrio Rizzuti, Tristan van Leeuwen, and Felix J. Herrmann. Adjoint operators enable fast and amortized machine learning based Bayesian uncertainty quantification. In Olivier Colliot and Ivana Išgum, editors, *Medical Imaging 2023: Image Processing*, volume 12464, page 124641L. International Society for Optics and Photonics, SPIE, 2023.
- [48] Antony Overstall and James McGree. Bayesian Decision-Theoretic Design of Experiments Under an Alternative Model. *Bayesian Analysis*, 17(4):1021 – 1041, 2022.
- [49] George Papamakarios, Eric Nalisnick, Danilo Jimenez Rezende, Shakir Mohamed, and Balaji Lakshminarayanan. Normalizing flows for probabilistic modeling and inference. *J. Mach. Learn. Res.*, 22(1), jan 2021.
- [50] Ben Poole, Sherjil Ozair, Aäron van den Oord, Alexander Amir Alemi, and G. Tucker. On variational bounds of mutual information. In *ICML*, 2019.
- [51] Dennis Prangle, Sophie Harbisher, and Colin S. Gillespie. Bayesian Experimental Design Without Posterior Calculations: An Adversarial Approach. *Bayesian Analysis*, 18(1):133 – 163, 2023.
- [52] Luc Pronzato and Andrej Pázman. Design of experiments in nonlinear models. *Lecture notes in statistics*, 212(1), 2013.
- [53] Jing Qin. Inferences for case-control and semiparametric two-sample density ratio models. *Biometrika*, 85(3):619–630, 1998.
- [54] Tom Rainforth, Robert Cornish, Hongseok Yang, and Andrew Warrington. On nesting Monte Carlo estimators. In *International Conference on Machine Learning*, pages 4267–4276. PMLR, 2018.
- [55] Danilo Rezende and Shakir Mohamed. Variational inference with normalizing flows. In Francis Bach and David Blei, editors, *Proceedings of the 32nd International Conference on Machine Learning*, volume 37 of *Proceedings of Machine Learning Research*, pages 1530–1538, Lille, France, 07–09 Jul 2015. PMLR.
- [56] Kenneth J Ryan. Estimating expected information gains for experimental designs with application to the random fatigue-limit model. *Journal of Computational and Graphical Statistics*, 12(3):585–603, 2003.
- [57] Filippo Santambrogio. *Optimal Transport for Applied Mathematicians: Calculus of Variations, PDEs, and Modeling*. Springer International Publishing, 2015.
- [58] Kathrin Smetana and Olivier Zahm. Randomized residual-based error estimators for the proper generalized decomposition approximation of parametrized problems. *International Journal for Numerical Methods in Engineering*, 121(23):5153–5177, 2020.
- [59] Alessio Spantini, Daniele Bigoni, and Youssef Marzouk. Inference via low-dimensional couplings. *Journal of Machine Learning Research*, 19(66):1–71, 2018.
- [60] Alessio Spantini, Antti Solonen, Tiangang Cui, James Martin, Luis Tenorio, and Youssef Marzouk. Optimal low-rank approximations of Bayesian linear inverse problems. *SIAM Journal on Scientific Computing*, 37(6):A2451–A2487, 2015.
- [61] Masashi Sugiyama, Taiji Suzuki, and Takafumi Kanamori. *Density Ratio Estimation in Machine Learning*. Cambridge University Press, 2012.

- [62] MTCAJ Thomas and A Thomas Joy. *Elements of information theory*. Wiley-Interscience, 2006.
- [63] Surya T Tokdar. Basic Probability Theory on Convergence. <http://www2.stat.duke.edu/~st118/sta732/convergence.pdf>.
- [64] Cédric Villani. *Optimal Transport: Old and New*, volume 338. Springer, 2009.
- [65] Stephen G. Walker. Bayesian information in an experiment and the fisher information distance. *Statistics & Probability Letters*, 112:5–9, 2016.
- [66] Sven Wang and Youssef Marzouk. On minimax density estimation via measure transport. *arXiv:2207.10231*, 2022.
- [67] Zheyu Oliver Wang, Ricardo Baptista, Youssef Marzouk, Lars Ruthotto, and Deepanshu Verma. Efficient neural network approaches for conditional optimal transport with applications in bayesian inference, 2024.
- [68] Jacob Westfall, David A. Kenny, and Charles M Judd. Statistical power and optimal design in experiments in which samples of participants respond to samples of stimuli. *Journal of experimental psychology. General*, 143 5:2020–45, 2014.
- [69] Christina Winkler, Daniel E Worrall, Emiel Hoogeboom, and Max Welling. Learning likelihoods with conditional normalizing flows. *arXiv:1912.00042*, 2019.
- [70] Keyi Wu, Peng Chen, and Omar Ghattas. A fast and scalable computational framework for large-scale high-dimensional Bayesian optimal experimental design. *SIAM/ASA Journal on Uncertainty Quantification*, 11(1):235–261, 2023.
- [71] Keyi Wu, Thomas O’Leary-Roseberry, Peng Chen, and Omar Ghattas. Large-scale Bayesian optimal experimental design with derivative-informed projected neural network. *Journal of Scientific Computing*, 95(1):30, 2023.
- [72] Olivier Zahm. *Model order reduction methods for parameter-dependent equations – Applications in Uncertainty Quantification*. PhD thesis, L’école Centrale Nantes, 11 2015.
- [73] Olivier Zahm, Tiangang Cui, Kody Law, Alessio Spantini, and Youssef Marzouk. Certified dimension reduction in nonlinear Bayesian inverse problems. *Mathematics of Computation*, 91(336):1789–1835, 2022.

**Appendix A. MLE and the second order delta method.** For completeness, we first state the multivariate second order delta method.

**Theorem A.1 (Second Order Delta Method).** *Let  $g: \mathbb{R}^p \rightarrow \mathbb{R}$  be a twice differentiable function at  $\alpha^*$  that satisfies  $\nabla g(\alpha^*) = 0$ . If  $r_N(\hat{\alpha}_N - \alpha^*) \xrightarrow{d} Z$ , where  $r_N \rightarrow \infty$  as  $N \rightarrow \infty$  and  $Z$  is a random variable in  $\mathbb{R}^p$  whose distribution is independent of  $N$ , then we have*

$$r_N^2(g(\hat{\alpha}_N) - g(\alpha^*)) \xrightarrow{d} \frac{1}{2} Z^\top \nabla^2 g(\alpha^*) Z.$$

From the theory of MLE and asymptotic normality, we have

$$\sqrt{N} (\hat{\alpha}_N - \alpha^*) \xrightarrow{d} \mathcal{N}(0, I^{-1}(\alpha^*)).$$

In addition, recall that  $g$  is defined as  $g(\alpha) = \mathbb{E}_{\pi_Y} [\log q_Y(y; \alpha)]$  and that  $\nabla g(\alpha^*) = 0$ . Applying Theorem A.1, we have that

$$N (g(\hat{\alpha}_N) - g(\alpha^*)) \xrightarrow{d} \frac{1}{2} Z^\top \nabla^2 g(\alpha^*) Z,$$

where  $Z \sim \mathcal{N}(0, I^{-1}(\alpha^*))$  in this case. We further note that the right hand side is the sum of Chi-square distributions. To be precise, let  $\{\lambda_i\}_{i=1}^p$  be the generalized eigenvalues of the matrix pencil  $(I(\alpha^*)^{-1}, (\nabla_\alpha^2 g(\alpha^*)))$ .

Then  $\mathbb{E} [N(g(\hat{\alpha}_N) - g(\alpha^*))]$  converges to  $\sum_{i=1}^p \lambda_i$ , and  $\mathbb{V} [N(g(\hat{\alpha}_N) - g(\alpha^*))]$  converges to  $2 \sum_{i=1}^p \lambda_i$  with the assumption that  $\mathbb{E} [N(g(\hat{\alpha}_N) - g(\alpha^*))^2] \leq C$  for some  $C$ . Please refer to Appendix C for more details.

**Appendix B. Proofs of the main results.**

*Proof of Theorem 2.3.* Recall that EIG can be computed as

$$\text{EIG} = \mathbb{E}_{\pi_{X,Y}} \left[ \log \frac{\pi_{Y|X}(y|x)}{\pi_Y(y)} \right].$$

This quantity can be estimated using samples, i.e.,  $\frac{1}{M} \sum_{i=1}^M \log \frac{\pi_{Y|X}(y^i|x^i)}{\pi_Y(y^i)}$ .

Suppose we can evaluate  $\pi_{Y|X}(y|x)$  exactly for any  $x$  and  $y$ , and suppose that the distribution is parametrized by  $\hat{\alpha}_N$ . Then the EIG estimator can be written as

$$\widehat{\text{EIG}}_{M,N} = \frac{1}{M} \sum_{i=1}^M \log \frac{\pi_{Y|X}(y^i|x^i)}{q_Y(y^i; \hat{\alpha}_N)},$$

whose bias is

$$\mathbb{E} \left[ \widehat{\text{EIG}}_{M,N} - \text{EIG} \right] = \mathbb{E}_{\pi_Y, \hat{\alpha}_N} \left[ \log \pi_Y(y) - \log q_Y(y; \hat{\alpha}_N) \right].$$

Let  $\alpha^*$  be the true parameter that generates the data. That is  $\pi_Y(y) = q_Y(y; \alpha^*)$ . We define

$$g(\alpha) := \mathbb{E}_{\alpha^*} \left[ \log q(y; \alpha) \right] = \mathbb{E}_{q_Y(y; \alpha^*)} \left[ \log q(y; \alpha) \right] = \mathbb{E}_{\pi_Y} \left[ \log q(y; \alpha) \right],$$

which is a function of  $\alpha$  only. Using Taylor expansion, we have

$$g(\hat{\alpha}_N) = g(\alpha^*) + \nabla g(\alpha^*)(\hat{\alpha}_N - \alpha^*) + \frac{1}{2}(\hat{\alpha}_N - \alpha^*)^\top \nabla^2 g(\alpha^*)(\hat{\alpha}_N - \alpha^*) + o_p(\|\hat{\alpha}_N - \alpha^*\|^2).$$

Here we also have  $\alpha^* = \arg \max_{\alpha} g(\alpha)$ , assuming that  $|\partial^3 g(\alpha)| \leq C$  for all  $\alpha$  [25]. Note that by the property of MLE,

$$\nabla g(\alpha^*) = 0.$$

Then using the asymptotic normality of MLE, we have that

$$\sqrt{N}(\hat{\alpha}_N - \alpha^*) \rightarrow \mathcal{N}(0, I(\alpha^*)^{-1})$$

where  $I(\alpha^*)$  is the Fisher information matrix, evaluated at  $\alpha^*$ . Since  $\nabla_{\alpha} g(\alpha^*) = 0$ , the Taylor expansion above can be written as

$$g(\hat{\alpha}_N) = g(\alpha^*) + \frac{1}{2}(\hat{\alpha}_N - \alpha^*)^\top \nabla_{\alpha}^2 g(\alpha^*)(\hat{\alpha}_N - \alpha^*) + o_p(\|\hat{\alpha}_N - \alpha^*\|^2).$$

Rearrange we have

$$\begin{aligned} N(g(\hat{\alpha}_N) - g(\alpha^*)) &= \frac{N}{2}(\hat{\alpha}_N - \alpha^*)^\top \nabla_{\alpha}^2 g(\alpha^*)(\hat{\alpha}_N - \alpha^*) + o_p\left(\left\|\sqrt{N}(\hat{\alpha}_N - \alpha^*)\right\|^2\right) \\ &= \frac{N}{2}(\hat{\alpha}_N - \alpha^*)^\top \nabla_{\alpha}^2 g(\alpha^*)(\hat{\alpha}_N - \alpha^*) + o_p(1), \end{aligned}$$

where we have used that  $\sqrt{N}(\hat{\alpha}_N - \alpha^*)$  converges in distribution, so  $\left\|\sqrt{N}(\hat{\alpha}_N - \alpha^*)\right\|^2 = O_p(1)$  and that  $o_p(O_p(1))$ . The first term on the right hand side converges to the weighted sum of Chi-square distributions with one degree of freedom  $\sum_{i=1}^p c_i \chi_{1_i}^2$  as  $N \rightarrow \infty$ , where we assume  $\alpha \in \mathbb{R}^p$ ,

and the limit is independent of  $N$ . (See Theorem A.1 and Appendix C). Note that the limiting distribution depends only on the dimension of  $\alpha^*$ , not the value of  $\alpha^*$ , thus fixed. We then have

$$g(\widehat{\alpha}_N) - g(\alpha^*) \xrightarrow{d} \frac{1}{N} \sum_{i=1}^p c_i \chi_{1_i}^2.$$

Let  $\mathbb{E} \left[ \sum_{i=1}^p c_i \chi_{1_i}^2 \right] = C_p$ , and assume  $g$  is a continuous and bounded function. Using Portmanteau theorem [63], we have that

$$\mathbb{E}_{\widehat{\alpha}_N} [g(\widehat{\alpha}_N)] - g(\alpha^*) \sim O(1/N).$$

We thus conclude that the bias converges at a rate of  $O(1/N)$ .

We then study the variance of  $\widehat{\text{EIG}}_{M,N}$ .

$$\begin{aligned} \mathbb{V} \left[ \widehat{\text{EIG}}_{M,N} \right] &= \mathbb{V} \left[ \frac{1}{M} \sum_{i=1}^M \log \pi_{Y|X}(y^i|x^i) - \frac{1}{M} \sum_{i=1}^M \log q_Y(y^i; \widehat{\alpha}_N) \right] \\ &= \mathbb{V} \left[ \frac{1}{M} \sum_{i=1}^M \log \pi_{Y|X}(y^i|x^i) \right] + \mathbb{V} \left[ \frac{1}{M} \sum_{i=1}^M \log q_Y(y^i; \widehat{\alpha}_N) \right] \\ &\quad - 2\text{Cov} \left[ \frac{1}{M} \sum_{i=1}^M \log \pi_{Y|X}(y^i|x^i), \frac{1}{M} \sum_{i=1}^M \log q_Y(y^i; \widehat{\alpha}_N) \right]. \end{aligned}$$

We then analyze each of the three terms separately. The term

$$\mathbb{V} \left[ \frac{1}{M} \sum_{i=1}^M \log \pi_{Y|X}(y^i|x^i) \right] = \frac{1}{M} \mathbb{V} \left[ \log \pi_{Y|X}(y|x) \right] \sim O(1/M),$$

as the samples are independent and the variance of  $\log \pi_{Y|X}(y|x)$  is a fixed quantity. To analyze  $\mathbb{V} \left[ \frac{1}{M} \sum_{i=1}^M \log q_Y(y^i; \widehat{\alpha}_N) \right]$ , we use the law of total variance:

$$\begin{aligned} \mathbb{V} \left[ \frac{1}{M} \sum_{i=1}^M \log q_Y(y^i; \widehat{\alpha}_N) \right] &= \frac{1}{M^2} \mathbb{V} \left[ \sum_{i=1}^M \log q_Y(y^i; \widehat{\alpha}_N) \right] \\ &= \frac{1}{M^2} \left( \mathbb{E}_{\widehat{\alpha}_N} \left[ \mathbb{V}_{\pi_Y} \left[ \sum_{i=1}^M \log q_Y(y^i; \widehat{\alpha}_N) \right] \right] + \mathbb{V}_{\widehat{\alpha}_N} \left[ \mathbb{E}_{\pi_Y} \left[ \sum_{i=1}^M \log q_Y(y^i; \widehat{\alpha}_N) \right] \right] \right) \\ &= \frac{1}{M^2} \left( M \mathbb{E}_{\widehat{\alpha}_N} \left[ \mathbb{V}_{\pi_Y} \left[ \log q_Y(y; \widehat{\alpha}_N) \right] \right] + M^2 \mathbb{V}_{\widehat{\alpha}_N} \left[ \mathbb{E}_{\pi_Y} \left[ \log q_Y(y; \widehat{\alpha}_N) \right] \right] \right) \\ &= \left( \frac{1}{M} \mathbb{E}_{\widehat{\alpha}_N} \left[ \mathbb{V}_{\pi_Y} \left[ \log q_Y(y; \widehat{\alpha}_N) \right] \right] \right) + \left( \mathbb{V}_{\widehat{\alpha}_N} \left[ \mathbb{E}_{\pi_Y} \left[ \log q_Y(y; \widehat{\alpha}_N) \right] \right] \right), \end{aligned}$$

where we have used the fact that  $\{\log q_Y(y^i; \widehat{\alpha}_N)\}_{i=1}^M$  are independent given  $\widehat{\alpha}_N$ . We then study two terms in the last equality separately. Define

$$f(\alpha) = \mathbb{V}_{\pi_Y} \left[ \log q_Y(y; \alpha) \right],$$

then

$$f(\hat{\alpha}_N) = f(\alpha^*) + \nabla_{\alpha} f(\alpha^*)(\hat{\alpha}_N - \alpha^*) + o_p\left(\|\hat{\alpha}_N - \alpha^*\|^2\right)$$

and

$$\mathbb{E}_{\hat{\alpha}_N} [f(\hat{\alpha}_N)] = f(\alpha^*) + \nabla_{\alpha} f(\alpha^*) \mathbb{E}_{\hat{\alpha}_N} [\hat{\alpha}_N - \alpha^*] + o_p\left(\mathbb{E}_{\hat{\alpha}_N} \|\hat{\alpha}_N - \alpha^*\|^2\right) \sim O(1).$$

For the second term, recall that  $g(\alpha)$  was previously defined as

$$g(\alpha) = \mathbb{E}_{\pi_Y} [\log q_Y(y; \alpha)] = \mathbb{E}_{a^*} [\log q_Y(y; \alpha)].$$

Using Portmanteau theorem again [63], we have that the second term

$$\mathbb{V}_{\hat{\alpha}_N} [\mathbb{E}_{\pi_Y} [\log q_Y(y; \hat{\alpha}_N)]] \sim O\left(\frac{1}{N^2}\right),$$

as we know that  $\mathbb{V}[N(g(\hat{\alpha}_N) - g(\alpha^*))] = N^2 \mathbb{V}(g(\hat{\alpha}_N))$  converge to the variance of the weighted sum of chi-square distribution as  $N$  goes to infinity, which is a constant. Therefore,

$$\mathbb{V} \left[ \frac{1}{M} \sum_{i=1}^M \log q_Y(y^i; \hat{\alpha}_N) \right] \sim O\left(\frac{1}{M} + \frac{1}{N^2}\right).$$

We then study the covariance term  $\text{Cov} \left( \frac{1}{M} \sum_{i=1}^M \log \pi_{Y|X}(y^i|x^i), \frac{1}{M} \sum_{i=1}^M \log q_Y(y^i; \hat{\alpha}_N) \right)$ . Note that  $\text{Cov} \left( \log \pi_{Y|X}(y^i|x^i), \log q_Y(y^j; \hat{\alpha}_N) \right) = 0$  for  $i \neq j$ . Therefore the expression can be simplified to

$$\frac{1}{M^2} \sum_{i=1}^M \text{Cov} \left( \log \pi_{Y|X}(y^i|x^i), \log q_Y(y^i; \hat{\alpha}_N) \right).$$

Using Cauchy-Schwarz, we have

$$\begin{aligned} & \text{Cov} \left( \log \pi_{Y|X}(y^i|x^i), \log q_Y(y^i; \hat{\alpha}_N) \right) \\ & \leq \sqrt{\mathbb{V} \left[ \log \pi_{Y|X}(y^i|x^i) \right] \mathbb{V} \left[ \log q_Y(y^i; \hat{\alpha}_N) \right]}. \end{aligned}$$

From previous analysis, the first term  $\mathbb{V} \left[ \log \pi_{Y|X}(y^i|x^i) \right]$  is a constant, and the second term  $\mathbb{V} \left[ \log q_Y(y^i; \hat{\alpha}_N) \right]$  converges at a rate of  $O(1 + \frac{1}{N^2})$  using the law of total variance. Therefore,

$$\frac{1}{M^2} \sum_{i=1}^M \text{Cov} \left( \log \pi_{Y|X}(y^i|x^i), \log q_Y(y^i; \hat{\alpha}_N) \right) \sim \frac{1}{M} O\left(1 + \frac{1}{N^2}\right) = O\left(\frac{1}{M}\right).$$

To conclude, we have

$$\begin{aligned} & \mathbb{V} \left[ \frac{1}{M} \sum_{i=1}^M \log \pi_{Y|X}(y^i|x^i) \right] \sim O\left(\frac{1}{M}\right), \\ & \mathbb{V} \left[ \frac{1}{M} \sum_{i=1}^M \log q_Y(y^i; \hat{\alpha}_N) \right] \sim O\left(\frac{1}{M} + \frac{1}{N^2}\right), \\ & \text{Cov} \left( \frac{1}{M} \sum_{i=1}^M \log \pi_{Y|X}(y^i|x^i), \frac{1}{M} \sum_{i=1}^M \log q_Y(y^i; \hat{\alpha}_N) \right) \sim O\left(\frac{1}{M}\right). \end{aligned}$$

Consequently,  $\mathbb{V} \left[ \widehat{\text{EIG}}_{M,N} \right] \sim O \left( \frac{1}{M} + \frac{1}{N^2} \right)$ . ■

*Proof of Theorem 2.6.* This theorem can be proved using the same techniques as in [proof](#), thus omitted. ■

*Proof of Theorem 2.7.* We first analyze the bias term,

$$\begin{aligned} & \mathbb{E} \left[ \widehat{\text{EIG}}_{M,N} - \text{EIG} \right] \\ &= \mathbb{E}_{\pi_Y, \widehat{\alpha}_N} \left[ \log \pi_Y(y) - \log q_Y(y; \widehat{\alpha}_N) \right] + \mathbb{E}_{\pi_{X,Y}, \widehat{\beta}_N} \left[ \log q_{Y|X}(y|x; \widehat{\beta}_N) - \log \pi_{Y|X}(y|x) \right]. \end{aligned}$$

Similar to the analysis in shown in the [proof](#) of Theorem 2.3, we have that the bias term converges at a rate of  $O(1/N)$ . We then analyze the variance term.

$$\begin{aligned} \mathbb{V} \left[ \widehat{\text{EIG}}_{M,N} \right] &= \mathbb{V} \left[ \frac{1}{M} \sum_{i=1}^M \log q_{Y|X}(y^i|x^i; \widehat{\beta}_N) - \frac{1}{M} \sum_{i=1}^M \log q_Y(y^i; \widehat{\alpha}_N) \right] \\ &= \mathbb{V} \left[ \frac{1}{M} \sum_{i=1}^M \log q_{Y|X}(y^i|x^i; \widehat{\beta}_N) \right] + \mathbb{V} \left[ \frac{1}{M} \sum_{i=1}^M \log q_Y(y^i; \widehat{\alpha}_N) \right] \\ &\quad - 2\text{Cov} \left( \frac{1}{M} \sum_{i=1}^M \log q_{Y|X}(y^i|x^i; \widehat{\beta}_N), \frac{1}{M} \sum_{i=1}^M \log q_Y(y^i; \widehat{\alpha}_N) \right). \end{aligned}$$

Recall from the previous [proof](#) that the first and the second term converge at a rate of  $O(1/M + 1/N^2)$ . For the covariance term, we use Cauchy-Schwarz and obtain

$$\begin{aligned} & \text{Cov} \left( \frac{1}{M} \sum_{i=1}^M \log q_{Y|X}(y^i|x^i; \widehat{\beta}_N), \frac{1}{M} \sum_{i=1}^M \log q_Y(y^i; \widehat{\alpha}_N) \right) \\ & \leq \sqrt{\mathbb{V} \left[ \frac{1}{M} \sum_{i=1}^M \log q_{Y|X}(y^i|x^i; \widehat{\beta}_N) \right] \mathbb{V} \left[ \frac{1}{M} \sum_{i=1}^M \log q_Y(y^i; \widehat{\alpha}_N) \right]}. \end{aligned}$$

We then know from the previous [proof](#) that both terms converge at a rate of  $O(1/M + 1/N^2)$ . Therefore, we conclude that

$$\mathbb{V} \left[ \widehat{\text{EIG}}_{M,N} \right] \sim O \left( \frac{1}{M} + \frac{1}{N^2} \right). \quad \blacksquare$$

*Proof of Corollary 2.8.* Suppose we have  $L$  samples in total, and let  $\gamma = \frac{M}{N}$ . We then get  $M = \frac{\gamma}{\gamma+1}L$  and  $N = \frac{1}{\gamma+1}L$ . We would then minimize  $\frac{A}{\gamma+1}L + \frac{B}{\frac{L^2}{(\gamma+1)^2}}$  over  $\gamma$ , where  $A, B$  are constants. We set the derivative of the above expression to 0 and get  $\frac{2\gamma^3 B + 2\gamma^2 B - AL}{\gamma^2 L^2} = 0$ . Solving for  $\gamma$ , we get  $\gamma = \frac{1}{3}(\zeta + \frac{1}{\zeta} - 1)$ , where  $\zeta = \frac{(3\sqrt{3}\sqrt{27A^2 B^4 L^2 - 8AB^5 L + 27AB^2 L - 4B^3})^{1/3}}{2^{2/3} B} \sim O(L^{1/3})$ . We see that if  $L$  is large, then  $\gamma \approx \frac{1}{3}(\zeta - 1)$ . Therefore, if we let  $L$  represent the total number of samples, the ratio of  $M$  to  $N$  should grow proportional to  $L^{1/3}$ . Using this optimal sample allocation, we obtain  $M = \frac{L}{L^{-1/3} + 1}$  and  $N = \frac{L}{L^{1/3} + 1}$ . Consequently, the MSE decays at a rate of  $\frac{2L^{2/3} + L + 2L^{1/3} + 1}{L^2}$ , with the dominant term being of the order  $L^{-1}$ . ■

**Appendix C. Chi-square distribution.** In this section we derive the mean and variance of the quadratic form  $(X - \mu)^\top \Sigma_2^{-1} (X - \mu)$  given a multivariate Gaussian random variable  $X \sim \mathcal{N}(\mu, \Sigma_1)$ .

**Theorem C.1.** *Suppose  $X \in \mathbb{R}^n$  is normally distributed, i.e.,  $X \sim \mathcal{N}(\mu, \Sigma_1)$ , then the random variable  $Y = (X - \mu)^\top \Sigma_2^{-1} (X - \mu)$  is the sum of Chi-square random variables, i.e.,  $(X - \mu)^\top \Sigma_2^{-1} (X - \mu) \sim \sum_{i=1}^n \lambda_i \chi_{1_i}^2$ , where  $\{\chi_{1_i}^2\}_{i=1}^n$  are independent Chi-square distributions with one degree of freedom and  $\lambda_i$ 's are the generalized eigenvalues of the matrix pencil  $(\Sigma_1, \Sigma_2)$ . Consequently, the mean and the variance of  $Y$  are  $\sum_{i=1}^n \lambda_i$  and  $2 \sum_{i=1}^n \lambda_i$ , respectively.*

*Proof.* Consider the matrix pencil  $(\Sigma_1, \Sigma_2)$ , with generalized eigenvalue  $\Lambda$  and eigenvector  $\Phi$ , where  $\Lambda$  is a diagonal matrix with eigenvalues being its diagonal entries and the corresponding eigenvector being the column of  $\Phi$ . We then have  $\Phi^\top \Sigma_1 \Phi = \Lambda$ ,  $\Phi^\top \Sigma_2 \Phi = I$ . Therefore,

$$\begin{aligned}\Sigma_1^{1/2} &= \Lambda^{1/2} \Phi^{-1} \\ \Sigma_2^{1/2} &= \Phi^{-1}.\end{aligned}$$

Since  $\Sigma_1^{-\top/2} (X - \mu) \sim \mathcal{N}(0, I)$ , plugging in  $\Sigma_1^{-\top/2} = \Lambda^{-1/2} \Phi^\top$ , we have

$$\Phi^\top (X - \mu) \sim \mathcal{N}(0, \Lambda),$$

from which we get

$$(X - \mu)^\top \Phi \Phi^\top (X - \mu) = (X - \mu)^\top \Sigma_2^{-1} (X - \mu) \sim \sum_{i=1}^n \lambda_i \chi_{1_i}^2.$$

The mean is  $\sum_{i=1}^n \lambda_i$ , and the variance is  $2 \sum_{i=1}^n \lambda_i$ . ■

### Appendix D. EIG estimates results of the linear elasticity inverse problem 4.3.

Table 1: Mean  $\pm$  2 standard error using CMI for dimension reduction

	$s = 1$	$s = 2$	$s = 3$	$s = 4$	$s = 5$	$s = 6$	$s = 7$	$s = 8$
$r = 1$	1.192 $\pm$ 0.294	1.786 $\pm$ 0.033	1.963 $\pm$ 0.039	2.005 $\pm$ 0.094	1.950 $\pm$ 0.087	1.941 $\pm$ 0.081	1.941 $\pm$ 0.081	1.941 $\pm$ 0.081
$r = 2$	1.761 $\pm$ 0.063	2.642 $\pm$ 0.073	2.942 $\pm$ 0.073	3.006 $\pm$ 0.154	2.956 $\pm$ 0.161	2.950 $\pm$ 0.172	2.952 $\pm$ 0.174	2.952 $\pm$ 0.174
$r = 3$	1.891 $\pm$ 0.341	3.050 $\pm$ 0.072	3.723 $\pm$ 0.111	3.946 $\pm$ 0.138	3.868 $\pm$ 0.167	3.864 $\pm$ 0.176	3.866 $\pm$ 0.179	3.866 $\pm$ 0.179
$r = 4$	1.864 $\pm$ 0.309	3.532 $\pm$ 0.123	4.325 $\pm$ 0.174	4.524 $\pm$ 0.239	4.557 $\pm$ 0.190	4.527 $\pm$ 0.178	4.504 $\pm$ 0.199	4.504 $\pm$ 0.199
$r = 5$	1.865 $\pm$ 0.313	3.552 $\pm$ 0.114	4.421 $\pm$ 0.179	4.625 $\pm$ 0.258	4.672 $\pm$ 0.202	4.651 $\pm$ 0.190	4.628 $\pm$ 0.209	4.627 $\pm$ 0.208
$r = 6$	1.871 $\pm$ 0.317	3.558 $\pm$ 0.109	4.644 $\pm$ 0.169	4.832 $\pm$ 0.239	4.894 $\pm$ 0.213	4.876 $\pm$ 0.203	4.854 $\pm$ 0.220	4.854 $\pm$ 0.220
$r = 7$	1.869 $\pm$ 0.317	3.569 $\pm$ 0.106	4.690 $\pm$ 0.166	4.935 $\pm$ 0.229	5.044 $\pm$ 0.184	5.029 $\pm$ 0.180	5.007 $\pm$ 0.198	5.007 $\pm$ 0.197
$r = 8$	2.042 $\pm$ 0.270	3.573 $\pm$ 0.106	4.691 $\pm$ 0.165	4.982 $\pm$ 0.237	5.094 $\pm$ 0.194	5.077 $\pm$ 0.187	5.050 $\pm$ 0.202	5.055 $\pm$ 0.205

Table 2: Mean  $\pm$  2 standard error using PCA for dimension reduction

	$s = 1$	$s = 2$	$s = 3$	$s = 4$	$s = 5$	$s = 6$	$s = 7$	$s = 8$
$r = 1$	0.575 $\pm$ 0.003	0.752 $\pm$ 0.002	1.014 $\pm$ 0.011	1.050 $\pm$ 0.014	1.082 $\pm$ 0.013	1.082 $\pm$ 0.013	1.083 $\pm$ 0.013	1.083 $\pm$ 0.013
$r = 2$	0.586 $\pm$ 0.003	0.898 $\pm$ 0.004	1.193 $\pm$ 0.011	1.294 $\pm$ 0.015	1.335 $\pm$ 0.019	1.343 $\pm$ 0.023	1.344 $\pm$ 0.023	1.344 $\pm$ 0.023
$r = 3$	0.844 $\pm$ 0.004	1.562 $\pm$ 0.008	1.986 $\pm$ 0.025	2.097 $\pm$ 0.053	2.138 $\pm$ 0.047	2.146 $\pm$ 0.054	2.147 $\pm$ 0.053	2.147 $\pm$ 0.053
$r = 4$	1.097 $\pm$ 0.004	1.816 $\pm$ 0.009	2.293 $\pm$ 0.030	2.362 $\pm$ 0.053	2.410 $\pm$ 0.052	2.418 $\pm$ 0.059	2.419 $\pm$ 0.059	2.419 $\pm$ 0.059
$r = 5$	1.142 $\pm$ 0.009	2.164 $\pm$ 0.014	2.631 $\pm$ 0.043	2.739 $\pm$ 0.056	2.787 $\pm$ 0.054	2.795 $\pm$ 0.060	2.796 $\pm$ 0.060	2.796 $\pm$ 0.060
$r = 6$	1.376 $\pm$ 0.013	2.413 $\pm$ 0.024	3.159 $\pm$ 0.049	3.179 $\pm$ 0.055	3.227 $\pm$ 0.052	3.234 $\pm$ 0.059	3.234 $\pm$ 0.058	3.234 $\pm$ 0.058
$r = 7$	1.375 $\pm$ 0.013	2.411 $\pm$ 0.024	3.158 $\pm$ 0.049	3.178 $\pm$ 0.055	3.226 $\pm$ 0.051	3.233 $\pm$ 0.059	3.233 $\pm$ 0.059	3.233 $\pm$ 0.059
$r = 8$	1.373 $\pm$ 0.013	2.414 $\pm$ 0.025	3.160 $\pm$ 0.050	3.260 $\pm$ 0.062	3.322 $\pm$ 0.063	3.329 $\pm$ 0.071	3.329 $\pm$ 0.070	3.329 $\pm$ 0.070

Table 3: Mean  $\pm$  2 standard error using CCA for dimension reduction

	$s = 1$	$s = 2$	$s = 3$	$s = 4$	$s = 5$	$s = 6$	$s = 7$	$s = 8$
$r = 1$	0.110 $\pm$ 0.021	0.114 $\pm$ 0.020	0.118 $\pm$ 0.020	0.118 $\pm$ 0.020	0.121 $\pm$ 0.019	0.121 $\pm$ 0.019	0.123 $\pm$ 0.019	0.123 $\pm$ 0.019
$r = 2$	0.111 $\pm$ 0.023	0.431 $\pm$ 0.035	0.434 $\pm$ 0.035	0.432 $\pm$ 0.035	0.439 $\pm$ 0.033	0.442 $\pm$ 0.033	0.445 $\pm$ 0.031	0.442 $\pm$ 0.032
$r = 3$	0.111 $\pm$ 0.023	0.440 $\pm$ 0.035	0.712 $\pm$ 0.058	0.712 $\pm$ 0.056	0.722 $\pm$ 0.055	0.728 $\pm$ 0.051	0.733 $\pm$ 0.049	0.735 $\pm$ 0.051
$r = 4$	0.111 $\pm$ 0.023	0.444 $\pm$ 0.035	0.715 $\pm$ 0.057	0.903 $\pm$ 0.060	0.915 $\pm$ 0.062	0.926 $\pm$ 0.056	0.933 $\pm$ 0.055	0.939 $\pm$ 0.055
$r = 5$	0.112 $\pm$ 0.023	0.445 $\pm$ 0.035	0.720 $\pm$ 0.058	0.910 $\pm$ 0.061	1.014 $\pm$ 0.054	1.030 $\pm$ 0.049	1.037 $\pm$ 0.048	1.041 $\pm$ 0.049
$r = 6$	0.110 $\pm$ 0.023	0.443 $\pm$ 0.035	0.719 $\pm$ 0.058	0.911 $\pm$ 0.061	1.018 $\pm$ 0.053	1.045 $\pm$ 0.051	1.052 $\pm$ 0.049	1.057 $\pm$ 0.050
$r = 7$	0.110 $\pm$ 0.022	0.442 $\pm$ 0.035	0.720 $\pm$ 0.057	0.912 $\pm$ 0.061	1.020 $\pm$ 0.053	1.048 $\pm$ 0.051	1.059 $\pm$ 0.050	1.063 $\pm$ 0.051
$r = 8$	0.110 $\pm$ 0.022	0.443 $\pm$ 0.034	0.720 $\pm$ 0.057	0.914 $\pm$ 0.062	1.021 $\pm$ 0.054	1.049 $\pm$ 0.052	1.060 $\pm$ 0.050	1.067 $\pm$ 0.052